Chapter 3

Metal Amidoboranes and Their Derivatives for Hydrogen Storage

Hailiang Chu, Shujun Qiu, Lixian Sun and Fen Xu

Additional information is available at the end of the chapter

http://dx.doi.org/10.5772/61048

Abstract

As potential hydrogen storage mediums, ammonia borane and its derivatives have been paid an increasing attention owing to their higher hydrogen capacities and facile dehydrogenation properties under moderate conditions. In this chapter, we presented extensive studies on thermodynamic tailoring of dehydrogenation of metal amidoboranes, metal borohydride-ammonia borane complexes, and metal amidoborane ammoniates as well as their derivatives, with special focus on the syntheses, crystal structures, and dehydrogenation properties. Finally, future perspective was given toward the practical applications.

Keywords: Hydrogen storage, dehydrogenation, metal amidoborane, B-N-containing compounds, thermodynamics, kinetics

1. Introduction

Mainly driven by two global issues of energy crisis and environmental pollution, great attention to a relatively new concept of the hydrogen economy has been paid in the last decades. However, hydrogen storage is one of bottlenecks in hydrogen economy. Generally, the materials with high hydrogen content have received an increasing interest for chemical storage concepts. As a chemical hydride, ammonia borane (NH_3BH_3, AB) has attracted significant attentions owing to the extremely high hydrogen capacity up to gravimetric density of 19.6 wt% and volumetric density of 146 g H_2 L^{-1} [1]. Unlike metal borohydrides, solid crystalline AB is not very sensitive to air at ambient condition. In AB molecules, there are both hydridic H atoms in BH_3 groups and protic H atoms in NH_3 groups. Consequently, the chemical potential of the interaction between protic $H^{\delta+}$ and hydridic $H^{\delta-}$ to the formation of hydrogen has been known as one of the prime driving powers for hydrogen release [2,3].

However, the relatively high kinetic barriers are observed in its multistep decomposition, which heightens the temperatures for hydrogen release more than 100 °C [4,5]. Other disadvantages of AB dehydrogenation consist of the discharge of some detrimental by-products (borazine and ammonia) and severe sample expansion and foaming. Moreover, the intrinsic exothermicity of dehydrogenation reveals that reversible hydrogenation under moderate conditions is thermodynamically impracticable. In recent years, a number of techniques including nanoconfinement [6-8], using ionic liquid medium [9], and catalytic modifications [10-14] were successfully employed in extensive studies. More importantly, another strategy proposed to improve the properties of AB thermolysis is the formation of metal-substituted AB-compounds, i.e., metal amidoboranes (MABs), which have been proven to be a practical method for tuning the dehydrogenation thermodynamics of AB [15-20]. Because of the quite high hydrogen content and reasonable dehydrogenation properties, this new type of materials has been paid intensive attention and grown to become one of the likeliest candidates for storing hydrogen.

In this chapter, we briefly summarize the recent progress of nanoconfinement and nanocatalysis of AB, metal amidoboranes (including single- and mixed-metal amidoboranes), and their derivatives (including metal amidoborane ammoniates, metal borohydride-ammonia borane complexes, and other complexes related to AB or MAB), with a particular emphasis on the synthesis, crystal structure, and dehydrogenation.

2. Nanoconfinement of AB

The pioneering work on AB nanoconfined in porous materials was performed by Autrey and his coworkers [6]. They loaded AB into SBA-15 (a kind of mesoporous material with specific surface area of about 900 $m^2\ g^{-1}$, pore size of 7.5 nm in diameter, and porous volume of 1.2 $cm^3\ g^{-1}$) by impregnating SBA-15 in a saturated methanol solution of AB. The obtained sample was determined to contain 50 wt% AB (denoted as AB:SBA-15). Compared to pristine AB, the sample nanoconfined in SBA-15 has two significant differences, as shown in Figure 1. First, the dehydrogenation peaks shifted to lower temperatures. Second, the great suppression of borazine evolution was successfully achieved, which indicates that the dehydrogenation reaction is probably tuned. The change of reaction pathway was further verified by differential scanning calorimetry (DSC) and nuclear magnetic resonance (NMR) experiments. From isothermal DSC test, the dehydrogenation reaction enthalpy of AB:SBA-15 was found to significantly reduce to 1 ± 1 kJ $(mol\ AB)^{-1}$, compared to pristine AB of 21 ± 1 kJ $(mol\ AB)^{-1}$. Also, NMR tests showed that the post-dehydrogenated product was only polyaminoborane (PAB) for AB:SBA-15 upon heating to 85 °C, which is different from pristine AB.

Isothermal dehydrogenation showed that the releasing rate of hydrogen from AB:SBA-15 was much more rapid than that from pristine AB. As an example, it needed less than 10 min for AB:SBA-15 to reach 50% reaction conversion at 80 °C, while 290 min for pristine AB. Also, a much lower activation energy of 67 ± 5 kJ mol^{-1} was determined for dehydrogenation from AB:SBA-15. However, the total amount of released hydrogen was undoubtedly sacrificed after AB loading into SBA-15, which was not specifically mentioned in their work.

http://dx.doi.org/10.5772/61048

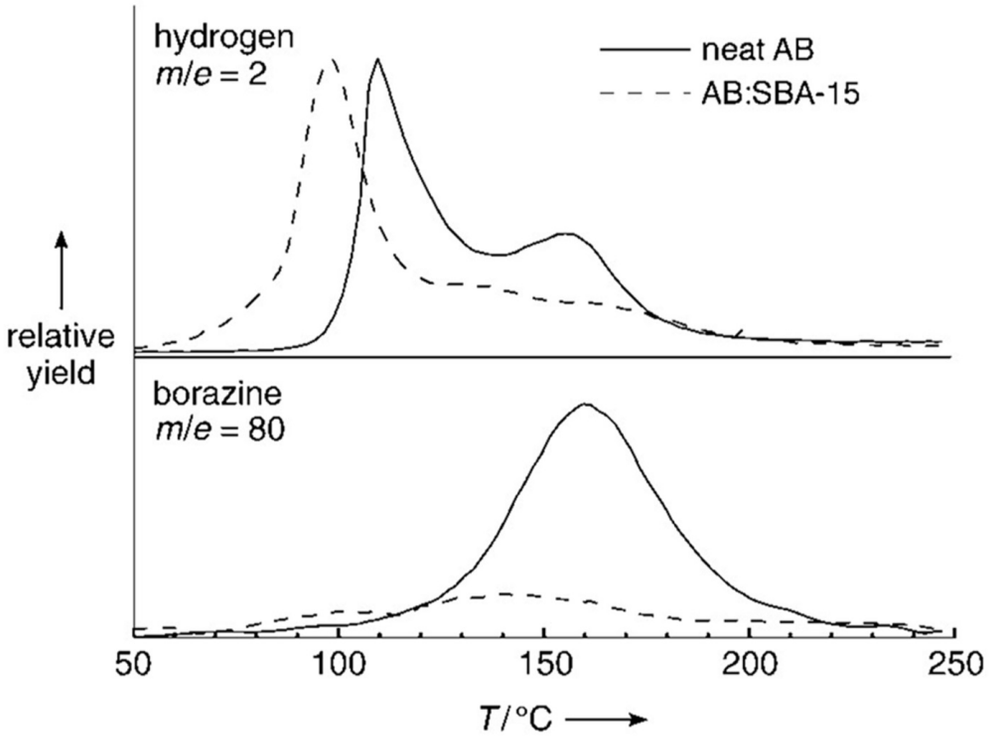

Figure 1. TPD/MS tests of AB nanoconfined in SBA-15 (AB:SBA-15). For comparison, neat AB was also included. Reproduced from Ref. [6] with permission.

In another study [7], carbon cryogel with specific surface area of 300 $m^2 g^{-1}$, pore diameter in the range of 2-20 nm, and pore volume of 0.7 $cm^3 g^{-1}$ was selected as a nanoscaffold to incorporate AB. Sample with a loading of 24 wt% AB into carbon cryogel was obtained (denoted as C−AB nanocomposite) by wet impregnation using tetrahydrofuran (THF) as solvent. Nitrogen physisorption test revealed that there is a loss of ~30% in pore volume after loading AB. From Figure 2, it was found that carbon cryogel as a nanoscaffold exhibited an even more pronounced effect on dehydrogenation than SBA-15. The peak for hydrogen release shifted to a low temperature of ~90 °C, and no signal for borazine was observed throughout the experiment. However, the total amount of released hydrogen was significantly less than that from pristine AB (9 wt% *vs.* 13 wt%). When confined in carbon cryogel, AB underwent the expected reactions for dehydrogenation. Unexpectedly, the enthalpy of dehydrogenation reaction for C−AB nanocomposite was determined to be an extremely high value of ~120 kJ mol^{-1} (compared to pristine AB of 21 ± 1 kJ mol^{-1} and AB:SBA-15 of 1 ± 1 kJ mol^{-1}). However, it remains so far unclear what caused the tremendous increase in reaction enthalpy. The authors suggested that the improvements (for AB loaded into both carbon cryogel and SBA-15) were ascribed to the increase of defect sites and surface energy of AB, resulting from nanoconfinement and/or the possible catalysis by the terminal SiO−H groups in SBA-15 and carboxylic groups in carbon cryogel. For carbon cryogel used as a nanoscaffold, the smaller the pore diameter, the lower the temperature for the dehydrogenation. In-depth studies of pore size effect on the structure and dehydrogenation are needed in the forthcoming research.

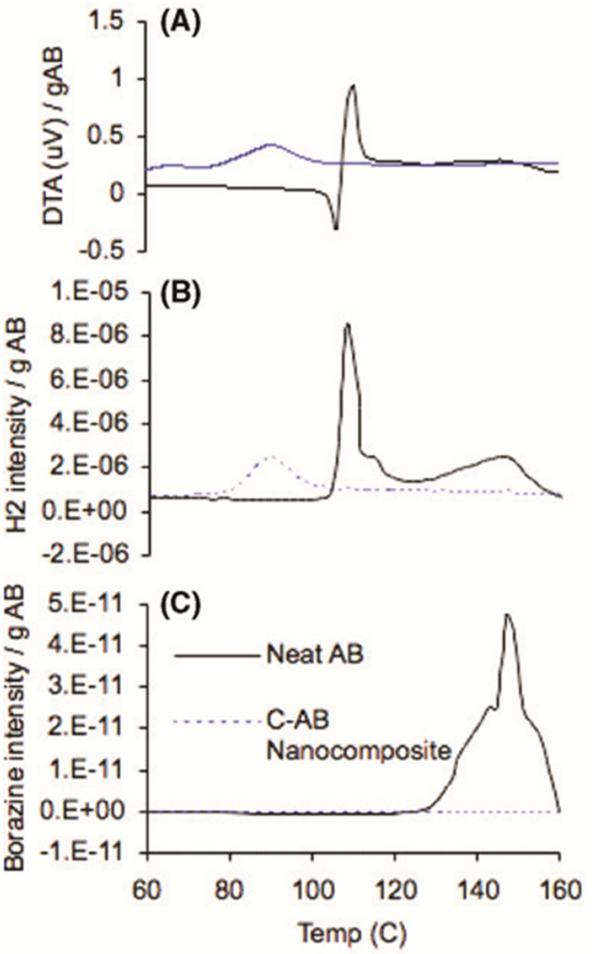

Figure 2. (A) DTA, MS for (B) H_2 and (C) borazine of AB nanoconfined in carbon cryogel (C-AB nanocomposite) at 1 °C/min. For comparison, neat AB was also included. Reproduced from Ref. [7] with permission.

As a newly developed kind of porous material, metal-organic frameworks (MOFs) consist of polydentate organic ligands and metal ions, achieving 3D extended frameworks [21,22]. A unique feature of MOFs is its adjustable porosity, which enables it with special properties like the combination of active metal sites and nanoporosity. Taking advantage of its porosity, an MOF-confined AB system was successfully synthesized by an infusion method using a solvent of methanol [23]. Y(BTC)(H_2O)·DMF (denoted as JUC-32-Y) was used as a nanoscaffold because of its high specific surface area, suitable pore size, and high thermal stability. Most importantly, it has many unsaturated metal sites after the removal of the terminal H_2O upon heating at 300 °C under vacuum (Figure 3A). After loading AB in 1:1 molar ratio, the framework of JUC-32-Y retained its integrity, even after dehydrogenation of AB/JUC-32-Y. Temperature programmed desorption coupled with mass spectrometry (TPD-MS) results shown in Figure 3B demonstrated that the dehydrogenation of AB/JUC-32-Y started at a lower temperature of ~50 °C, with a peak at 84 °C for most rapid releasing rate, which has a reduction of 30 °C in comparison with pristine AB. Furthermore, no volatile products such as B_2H_6, NH_3, and borazine were detected during the decomposition process. The suppression of ammonia was

http://dx.doi.org/10.5772/61048

ascribed to the existence of unsaturated coordination of Y^{3+}. Figure 3C indicates a notable improvement of the dehydrogenation kinetics of AB/JUC-32-Y. At 95 °C, 10.2 wt% H_2 could be released in initial 10 min while 8.0 wt% H_2 at a reduced temperature of 85 °C. Pristine AB displayed no emission of any hydrogen under same conditions. Note that AB/JUC-32-Y could release ~13 wt% H_2 at 95 °C within 3 h, corresponding to 2 Eq of H_2 in pristine AB.

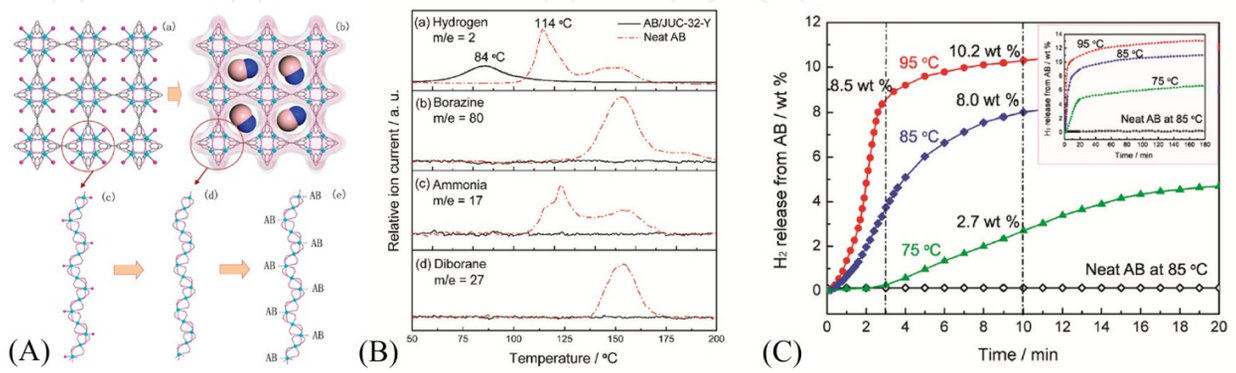

Figure 3. (A) 3D images of (a) JUC-32-Y and (b) AB/JUC-32-Y. Views of 1D chains of JUC-32-Y (c) before and (d) after removal of terminal H_2O and (e) after interaction with AB. Y: bright blue; C: gray; O: pink; N: blue; and B: purple. (B) TPD-MS and (C) Isothermal dehydrogenation of AB/JUC-32-Y. For comparison, neat AB was also included. Reproduced from Ref. [23] with permission.

Soon afterward, Gadipelli et al. [24] reported the confinement of AB in Mg-MOF-74 with 1D pores (denoted as AB/Mg-MOF-74), in which the dehydrogenation kinetics had a remarkable improvement under 100 °C. Furthermore, in the released hydrogen, the detrimental concomitants such as ammonia, borazine, and diborane were not detectable throughout the dehydrogenation process. More importantly, owing to the relatively high specific surface area of 1100 $m^2\ g^{-1}$ and low atomic weight of metal cation, Mg-MOF-74 could contain about 26 wt% AB determined by theoretically structural optimization, while only about 8 wt% AB in JUC-32-Y [23]. Almost 14 wt% of pure H_2 could be released at a temperature of 125 °C in one hour for the AB/Mg-MOF-74 sample, which exceeded 13 wt% of H_2 (2 Eq) from pristine AB. Further systematic investigation showed that the dehydrogenation kinetics of AB/Mg-MOF-74 were very dependent on the loading amount of AB. Other MOFs such as Ni-MOF-74 and HKUST-1 were also tried in this work. However, the structures collapsed with AB loading, which enabled them to be unsuitable for serving as a nanoscaffold. In our related study [25], new tactics for loading AB in MIL-101 (AB/MIL-101) or Ni-modified MIL-101 (AB/Ni@MIL-101) were proposed through wet impregnation. As shown in Figure 4, the dehydrogenation of AB/MIL-101 proceeded without an induction period or any detectable borazine and diborane, but with some ammonia. For the case of AB/Ni@MIL-101, the dehydrogenation peak for the most rapid rate was reduced to a lower temperature of 75 °C. Furthermore, the detrimental by-products of borazine, diborane, and ammonia were not detected during the whole experiments. Theoretical calculations indicated the establishment of B–O and Cr–N bonds and the existence of strong interaction between MIL-101 and NH_2BH_2 species, which could facilitate the dehydrogenation.

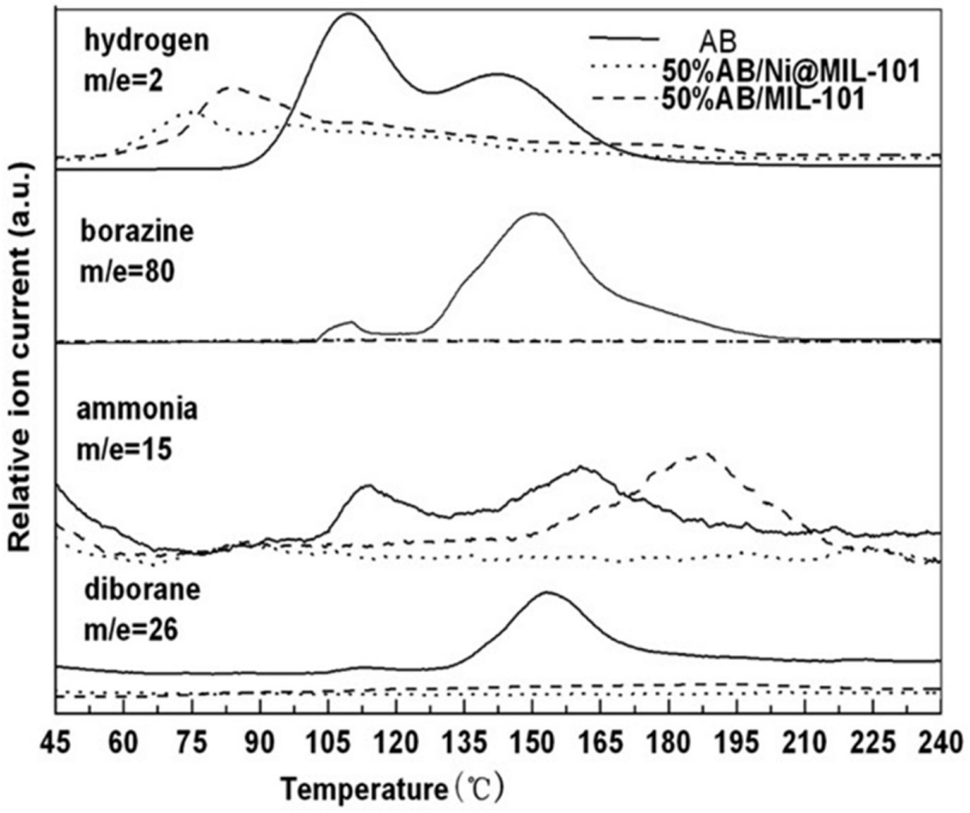

Figure 4. TPD-MS of AB, AB/Ni@MIL-101, and AB/MIL-101. Reproduced from Ref. [25] with permission.

3. Nanocatalysis of AB

$Ni_{1-x}Pt_x$ (x = 0-0.12) hollow spheres were prepared with an assistance of a template called as poly(styrene-co-methacrylic acid) and then used as catalysts for generating hydrogen from AB [26]. The morphology and the composition of the obtained $Ni_{0.88}Pt_{0.12}$ sample were shown in Figure 5. There are both broken and intact hollow spheres appeared in the sample. TEM images revealed that the porous shells of hollow spheres with a thickness of 20-40 nm contained many smaller nanowhiskers and nanoparticles, which enabled the increase of specific surface area of hollow spheres. Then the hollow spheres with a chemical composition of $Ni_{0.88}Pt_{0.12}$ were introduced into a methanol solution of AB. The mixture was vacuumed to obtain a dry solid sample with homogeneous loading of about 1.8 wt% Pt. TPD tests in Figure 6 showed that the onset temperature for hydrogen release was reduced to about 56 °C and the peak shifted to about 100 °C.

A "co-precipitation" process was developed using a typical wet-chemical method for fabricating nanoalloy to catalyze AB dehydrogenation [27]. Typically, a mixture of 2.0 mol % of $CoCl_2$ and 10 mL of THF was stirred by ultrasound at room temperature. Then AB was introduced into the resultant THF solution, which was immediately distilled under a

http://dx.doi.org/10.5772/61048

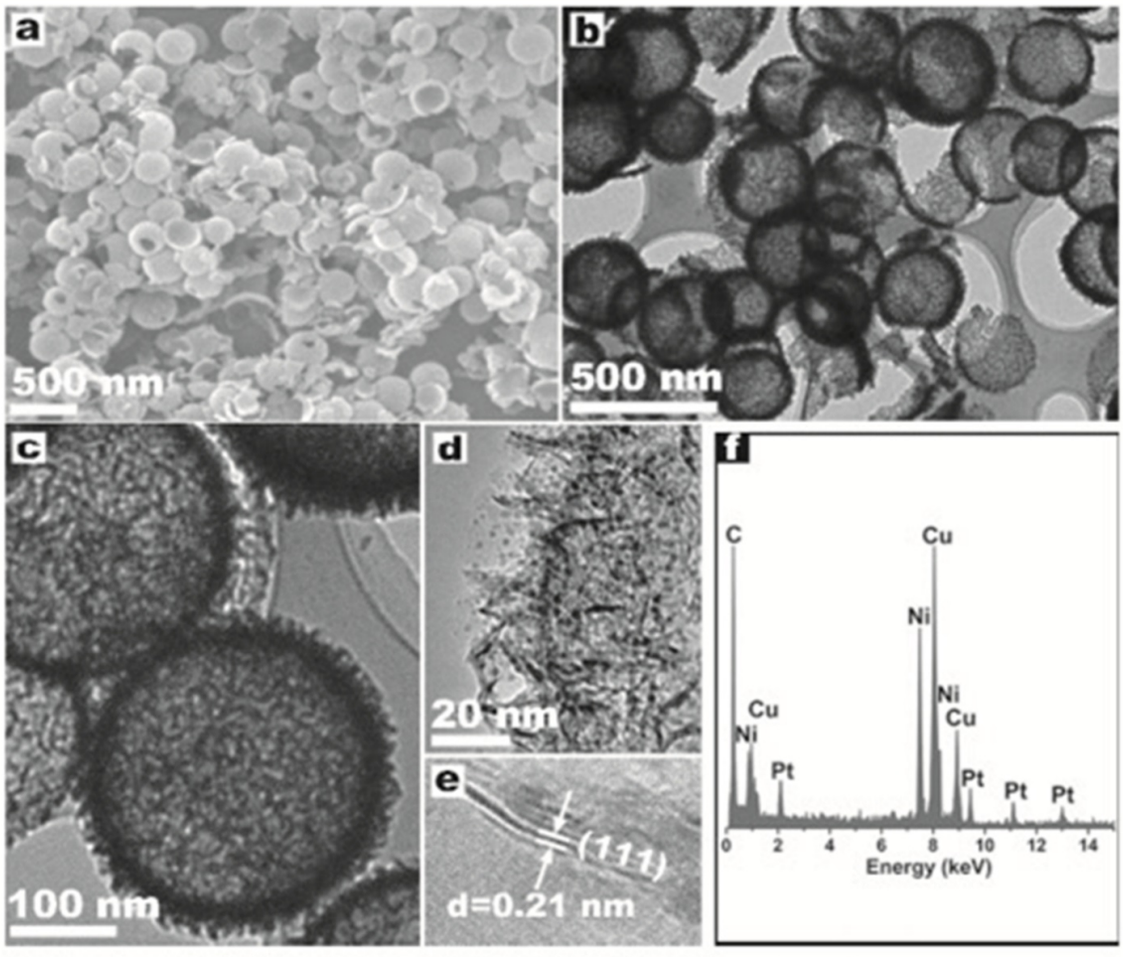

Figure 5. (a) SEM image, (b, c, d) TEM images, and (e) HRTEM image and (f) EDX spectrum of $Ni_{0.88}Pt_{0.12}$ hollow spheres. Reproduced from Ref. [26] with permission.

reduced pressure at room temperature. Finally, the Co-doped sample was obtained after continuous evacuation to eliminate the rest of THF. Ni-doped sample could be prepared in the same way. The size of most Ni and Co particles was below 3 nm, which indicated the peculiarity of the "co-precipitation" method in synthesizing nanoscaled metal catalysts. TPD-MS curves in Figure 7A showed that the catalyst-doped AB started to release H_2 at a very low temperature of 50 °C and exhibited broad dehydrogenation processes peaked at about 113 °C. Isothermal dehydrogenation test indicated that nearly 1 Eq of H_2 was released from the catalyst-doped AB at 59 °C without any induction period (Figure 7B). However, after being held at this temperature for more than 24 h, there was no evolution of any H_2 from pristine AB. Moreover, the detrimental by-product of borazine and sample forming were not observed during the catalytic dehydrogenation. Determined by the Kissinger model, the activation energy E_a was reduced to 117 and 123 kJ mol^{-1} for Co- and Ni-doped AB. For the case of Co-doped AB, from electron paramagnetic resonance (EPR) characterization, Co^{2+} was partially reduced in the preparation, which was regarded as the catalytically active species for AB dehydrogenation.

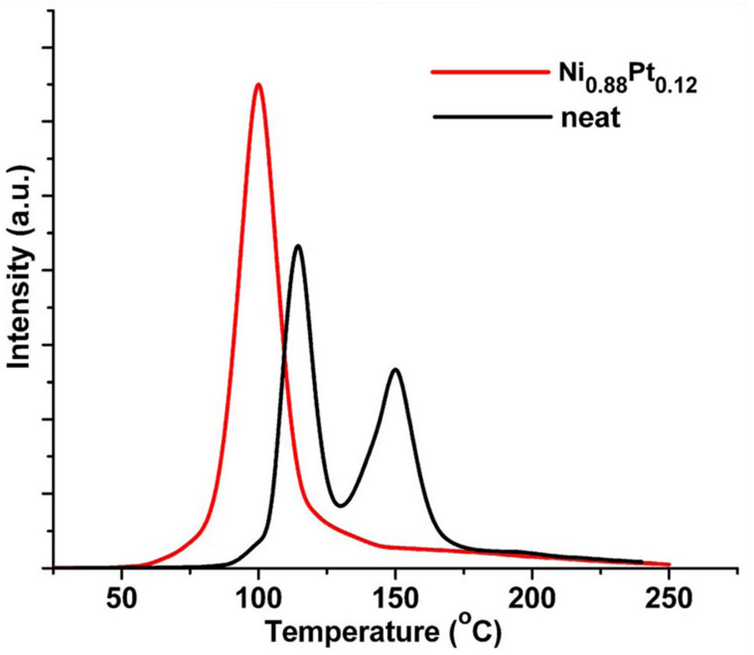

Figure 6. TPD-MS of AB mixed with $Ni_{0.88}Pt_{0.12}$ hollow spheres (red line). For comparison, neat AB (black line) was also included. Reproduced from Ref. [26] with permission.

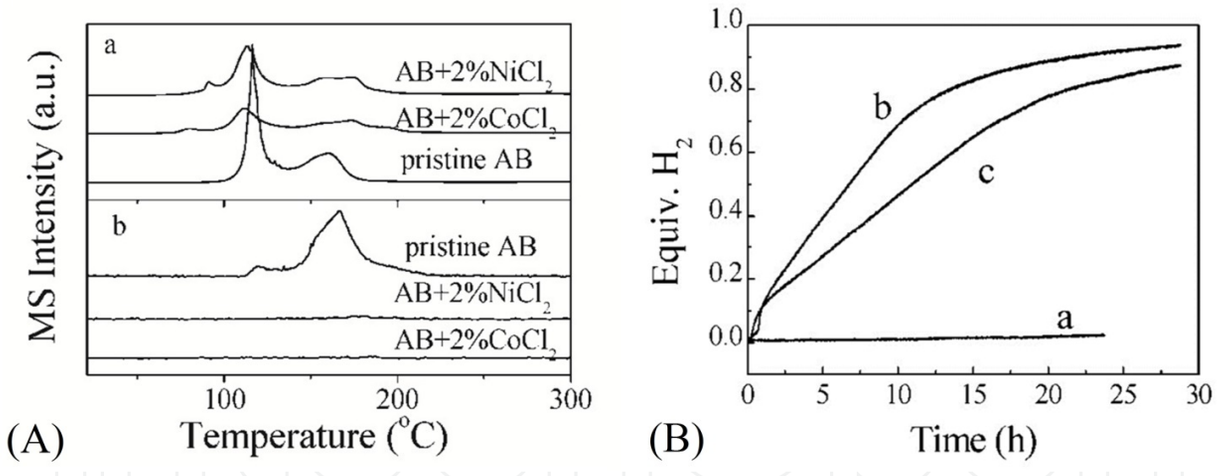

Figure 7. (A) TPD-MS of pristine and 2.0 mol% Co- or Ni-doped AB samples: (a) H_2 signal and (b) borazine signal. (B) Isothermal hydrogen release tests at 59 °C on (a) pristine, (b) Co-doped, and (c) Ni-doped AB samples. Reproduced from Ref. [27] with permission.

Because the chlorides of cobalt and nickel as precursors have better performance in catalyzing the dehydrogenation of AB, $FeCl_3$ and $FeCl_2$ were tried in the following studies [28,29]. Different amounts of $FeCl_3$ or $FeCl_2$ were introduced in solid AB using a "co-precipitation" method. Generally, $FeCl_3$ exhibited much better performance in catalyzing AB dehydrogenation than $FeCl_2$. Because of the formation of FeB nanoalloy in particle size of 2-5 nm, AB doped with 5 mol% $FeCl_3$ gave excellent performance with an onset temperature for hydrogen release

http://dx.doi.org/10.5772/61048

at about 55 °C. Volumetric release tests (Figure 8) showed that $FeCl_3$-doped AB evolved H_2 immediately at 60 °C without an induction period observed. With the increase of temperature to 80 °C and 100 °C, it could release more than 1.2 and 1.5 Eq of H_2, respectively. Also, sample foaming upon heating and the by-products (borazine and ammonia) were significantly suppressed. More importantly, crystalline linear polyaminoborane (PAB) was found upon dehydrogenation of $FeCl_3$-doped AB, which was the first case on the preparation of crystalline PAB through solid-state reaction. Theoretical calculations showed that the growth of crystalline PAB may follow the dehydrogenation-chain growth mechanism. When the loading amount of $FeCl_3$ was reduced to 2.0 mol%, the optimal performance of the formation of crystalline PAB was achieved.

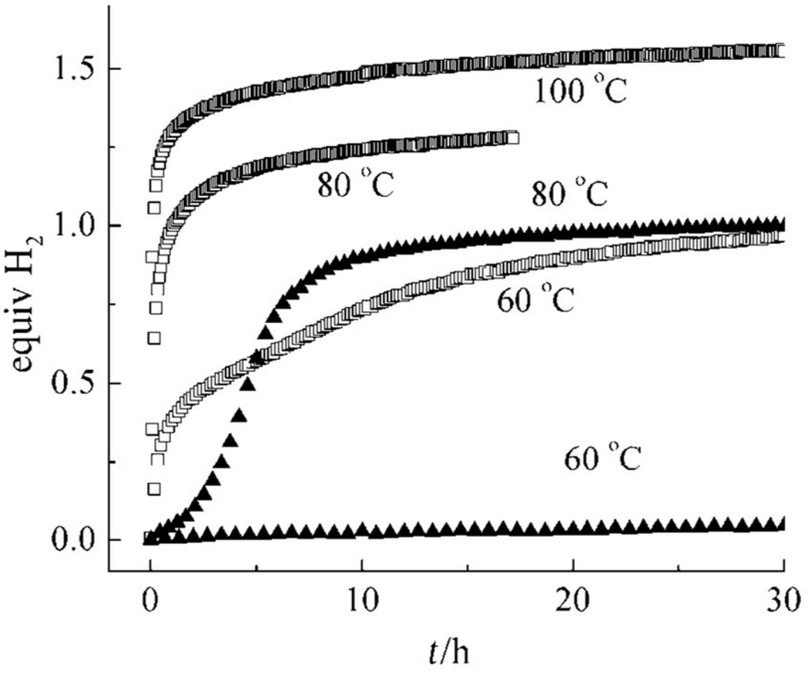

Figure 8. Volumetric release of 5.0 mol% $FeCl_3$-doped AB samples (□). For comparison, pristine AB (▲) was also included as a reference. Reproduced from Ref. [28] with permission.

As shown in Figure 9, a nanocomposite of AB/Li-CMK-3 was successfully synthesized by an impregnation method, i.e., AB loaded into a Li-doped CMK-3 (a class of carbon material with an ordered mesoporous structure) [30]. It could release more than 7 wt% H_2 at 60 °C, which was ascribed to the synergy between catalytic effect and nanoconfinement in AB/Li-CMK-3 system. These effects resulted in a significant enhancement of the dehydrogenation kinetics and a great suppression of detrimental by-products. In reference [31], two novel catalysts based on MOFs (denoted as MOF1cat and MOF2cat) were developed, in which in situ-formed metal Ni and the retained frameworks greatly promoted their catalytic activity. Loading with only 1.0 mol% catalyst in AB would give rise to higher dehydrogenation capacity, more rapid hydrogen releasing rates, lower onset temperature, and much less reaction exothermicity. At 90 °C, about 8 wt% H_2 could be released from catalyzed samples. The reaction enthalpies of

AB dehydrogenation catalyzed by MOF1cat and MOF2cat were determined to be −4.3 and −7.9 kJ mol^{-1}, respectively, much less than −21 kJ mol^{-1} for pristine AB. The apparent activation energies of 131 and 160 kJ mol^{-1} were also much lower than 184 kJ mol^{-1} for pristine AB.

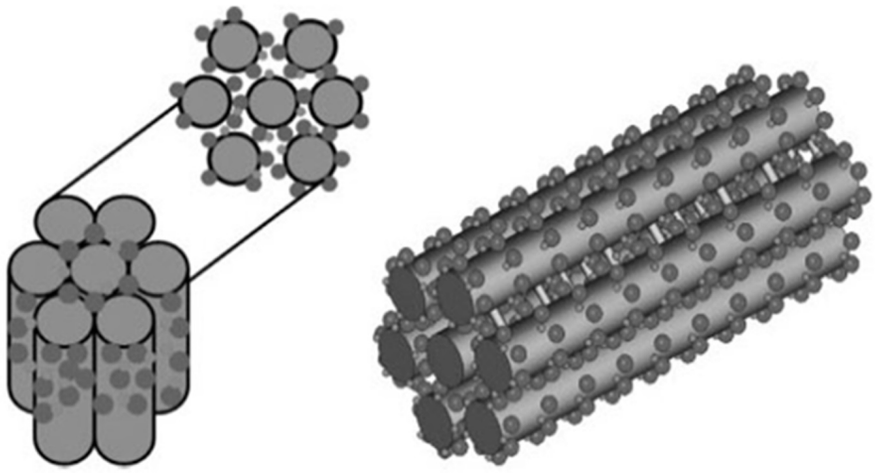

Figure 9. Schematic model of AB/Li-CMK-3 nanocomposites (AB: dark gray spheres; Li: light gray spheres; CMK-3 substrate: gray rod). Reproduced from Ref. [30] with permission.

Other catalysts consisting of noble metals were fabricated. For instance, the catalytic dehydrogenation properties of AB by carbon nanotubes functionalized with Pt nanoparticles (denoted as Pt@CNTs) were reported, in which Pt@CNTs was synthesized through an "ammonia-deliquescence" method [32]. From Figure 10, AB/Pt@CNTs had two peaks for hydrogen release at temperatures of about 108 °C and 150 °C. Furthermore, great suppression of borazine and no sample foaming and expansion were observed during the whole dehydrogenation. Of particular concern is achieving much less exothermicity for dehydrogenation. Meanwhile, AB/Pt@CNT had ameliorative dehydrogenation kinetics, i.e., releasing 1 Eq of H_2 in 5 h at 70 °C, which was evidenced by the reduced activation energy of 106.2 kJ mol^{-1}. It was also indicated that the combination of the nanoconfinement of AB into CNTs and the synergetically catalytic effects of Pt nanoparticles and CNTs were primarily responsible for enhancing the dehydrogenation properties. In addition, Pd, Pt, and Ni nanoparticles well deposited on MCM-48 (a silica-based material with mesoporous structure) were developed by a magnetron sputtering technique [33]. Then the resultant catalysts were introduced into AB by impregnation method using anhydrous diethyl ether as solvent and displayed obvious catalytic effects for hydrogen release from AB. For example, the onset temperature for dehydrogenation was about 93 °C for AB/MCM-48-Pd (weight ratio of 2:1), with a shift of 12 °C to reduced temperature compared with pristine AB. For all samples catalyzed by well-dispersed Pd, Pt, and Ni nanoparticles on MCM-48, borazine as a detrimental by-product was significantly suppressed, and there was no foaming and expansion during dehydrogenation process.

http://dx.doi.org/10.5772/61048

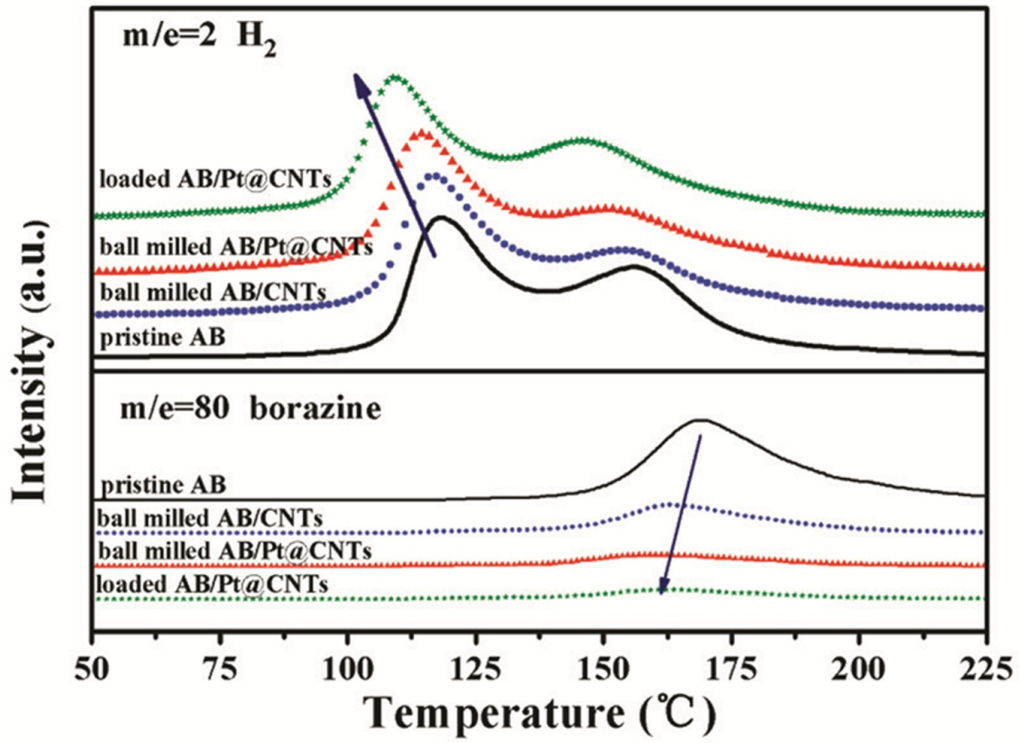

Figure 10. TPD-MS of pristine AB and loaded AB/Pt@CNTs. Reproduced from Ref. [32] with permission.

4. Metal amidoboranes, MABs

In 1938, sodium amidoborane ($NaNH_2BH_3$, NaAB, similarly hereinafter for other amidoboranes) was initially prepared by a reaction of borane etherate with sodium and ammonia [34]. For the case of lithium amidoborane ($LiNH_2BH_3$, LiAB), it was synthesized through deprotonation of AB in THF using *n*-butyllithium at 0 °C and then used as a reducing reagent [35]. However, the crystal structure of LiAB and NaAB was not reported until 2008 [36-38]. A solid-state synthetic method was developed for MABs through controlled mechanical ball milling AB with MH (M = Li or Na) in an equivalent molar amount. Calcium amidoborane ($Ca(NH_2BH_3)_2$, CaAB) was prepared by a wet-chemical reaction between AB and CaH_2 in THF [39]. As a matter of fact, CaAB·2THF rather than pure CaAB was obtained in final product due to the strong coordination of THF with Ca^{2+}. Wu et al. [38] synthesized solvent-free CaAB by ball milling solid-state CaH_2 and AB. More recently, some new MABs such as potassium amidoborane (KNH_2BH_3, KAB) [40], strontium amidoborane ($Sr(NH_2BH_3)_2$, SrAB) [41], and yttrium amidoborane ($Y(NH_2BH_3)_3$, YAB) [42] were successfully synthesized. In general, there are two synthetic approaches for the preparation according to the reported MABs, i.e., solid-state mechanical ball milling and wet-chemical synthesis. In solid-state ball milling method, the chemical interaction between protic H and hydridic H was regarded as one of main driving forces for hydrogen release [43-45]. It should be pointed out that the milling conditions are

crucial during the synthesis of MABs because of their lower temperatures for dehydrogenation. In a wet-chemical reaction, the adducts rather than pure MABs are always obtained because the solvent is easily coordinated with amidoborane, especially alkaline-earth metal amidoboranes [39]. Because of relatively strong combination between solvent molecules and metal cations, special procedures are needed for removal of solvent, during which the decomposition of MABs should be avoided.

4.1. Lithium amidoborane ($LiNH_2BH_3$, LiAB) and sodium amidoborane ($NaNH_2BH_3$, NaAB)

As mentioned above, LiAB or NaAB could be prepared by carefully milling a mixture of AB and an equivalent LiH or NaH. LiAB crystallizes in an orthorhombic cell (space group *Pbca*) with lattice parameters of a = 7.11274(6) Å, b = 13.94877(14) Å, and c = 5.15018(6) Å (Figure 11) [36]. Moreover, NaAB is an isostructural compound with LiAB and the lattice parameters are a = 7.46931(7) Å, b = 14.65483(16) Å, and c = 5.65280(8) Å [36]. In their crystal structures, the bond lengths of Na-N and Li-N are 2.35 and 1.98 Å. The substitution of one H atom in NH_3 group by Li^+ gave rise to the slight shortening of bond length for B-N (1.56 Å) compared to that in AB (1.58 Å) [46]. Moreover, the B-H distance is 1.079 Å in LiAB and 1.245 Å averagely in NaAB, which are different from that that in AB (1.11 Å) [47]. The establishment of an ionic Li-N or Na-N bond and the resulting reinforce of B-N bond in $[NH_2BH_3]^-$ group in LiAB or NaAB resulted in an improved dehydrogenation properties. LiAB and NaAB started to release H_2 at 85 °C and had a peak at about 90 °C [36,37]. In addition, no borazine was detectable during the dehydrogenation. Furthermore, the heat for dehydrogenation from LiAB and NaAB was determined to be ~-3 and -5 kJ (mol H_2^{-1}), remarkably less exothermic than that of pristine AB (-21 kJ (mol H_2^{-1})) [4]. At 91 °C, about 7.4 and 11 wt% H_2 could be released from NaAB and LiAB, respectively (Figure 12).

LiAB could also be synthesized by reaction of LiH and AB in THF after the evolution of 1 Eq of H_2. Surprisingly, it then releases another 2 Eq of H_2 in THF at a lowest temperature of 40 °C reported so far [48]. The dehydrogenation of LiAB in THF was determined to be zero-order based on the concentration of LiAB. However, the dehydrogenation mechanism is still unclear and needs further investigations. Through an electrospinning technique, LiAB nanoparticles were well dispersed in carbon nanofibers (denoted as LiAB@CNFs), which had onset and peak temperatures of about 40 °C and 80 °C, significantly lower than pristine LiAB. Upon heating to 100 °C, all hydrogen in LiAB of 10.6 wt% could be released in only 15 min [49]. For the case of NaAB, it could also be prepared through a wet-chemical method by reacting AB with NaH at -3 °C or with $NaNH_2$ at 25 °C in THF [50]. After dehydrogenation of LiAB or NaAB, the solid residues were found to be poorly crystalline phases. A following study indicated that solid NaH was detected for NaAB [50]. However, a recent investigation on the post-dehydrogenated products of NaAB at 200 °C suggested that except NaH, an amorphous phase with the chemical composition of $Na_{0.5}NBH_{0.5}$ (or regarded as a mixture of NaNBH and *h*-BN) was identified by NMR technique [51]. Unfortunately, the results from Fijałkowski et al. [52] showed that a substantial amount of NH_3 was released during synthesis by ball milling and the following thermal decomposition of NaAB.

http://dx.doi.org/10.5772/61048

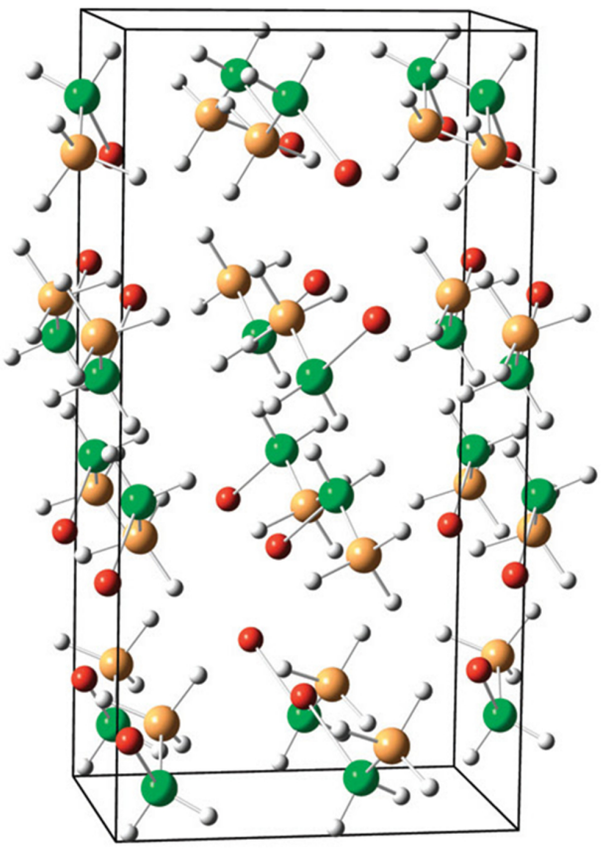

Figure 11. Crystal structure of LiAB. B: orange spheres; N: green spheres; H: white spheres; and Li: red spheres. Reproduced from Ref. [36] with permission.

4.2. Lithium amidoborane-ammonia borane ($LiNH_2BH_3 \cdot NH_3BH_3$, LiAB·AB) and β-LiAB

Careful exploration by XRD technique during ball milling of AB and LiH (in 1:1 molar ratio) indicated a stepwise process in LiAB formation [53]. A new complex hydride of lithium amidoborane-ammonia borane ($LiNH_2BH_3 \cdot NH_3BH_3$, LiAB·AB) was formed as an intermediate [38,53]. Pure LiAB·AB could be prepared by ball milling a mixture of AB/LiAB or 2AB/LiH [54]. It crystallizes in a monoclinic cell (space group $P21/c$) with lattice parameters of a = 7.0536(9) Å, b = 14.8127(20) Å, c = 5.1315(7) Å, and β = 97.491(5)°. There is the intergrowth of AB and LiAB layers in crystal structure of LiAB·AB. As shown in Figure 13, each Li^+ is bonded with one N atom from $[NH_2BH_3]^-$ with a Li-N bond in 2.05 Å and coordinated with hydrogen atoms from BH_3 group in two LiAB and one AB. The dihydrogen bonding of NH···HB is 1.902 Å in AB layer. About 14.0 wt% H_2 could be released at 228 °C from LiAB·AB after its melting with an onset temperature of 58 °C. Furthermore, another allotrope of β-LiAB was found during ball milling process. Interestingly, it transformed from initially formed α-LiAB and could transform to α-LiAB upon extended milling [53]. β-LiAB also crystallizes in an orthorhombic cell (space group $Pbca$) with lattice parameters of a = 15.15 Å, b = 7.726 Å, and c = 9.274 Å. However, its unit cell has a double volume of α-LiAB, in which two alternative LiAB layers were observed along the a axis. The coordination of Li^+ was found to be distortedly tetrahedral

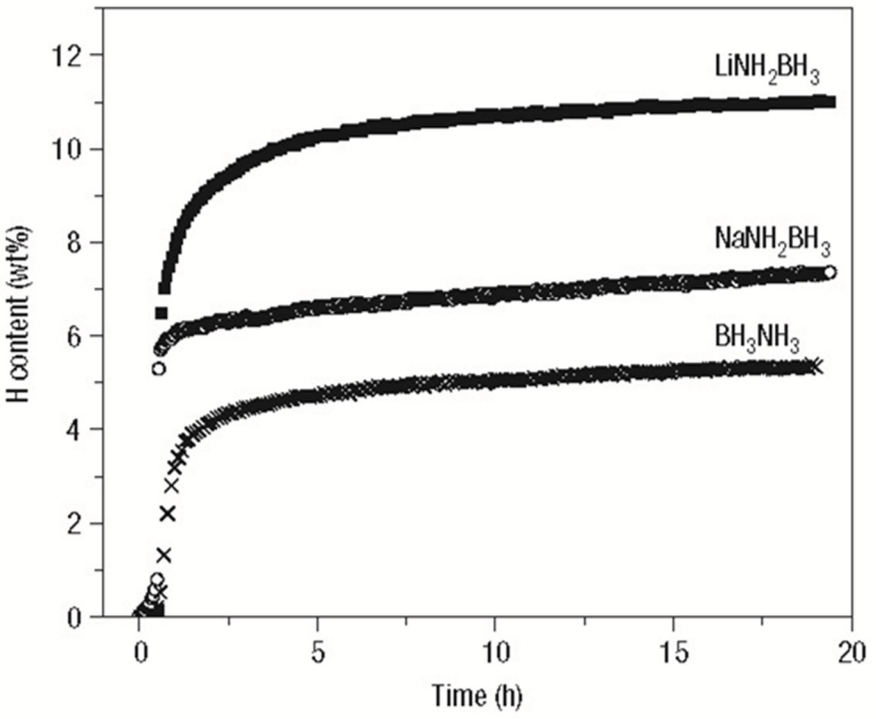

Figure 12. Isothermal dehydrogenation of LiAB, NaAB, and post-milled AB samples at about 91 °C. Reproduced from Ref. [36] with permission.

in β-LiAB due to different distances for Li1-B and Li2-B (Figure 13b). The bond length of Li-N (1.93 and 2.04 Å for Li1-N and Li2-N) is similar to that in α-LiAB (1.98 [36] or 2.02 Å [53]). Both allotropes of LiAB displayed identical dehydrogenation behaviors, i.e., 10.8 wt% H_2 could be released at 180 °C [53].

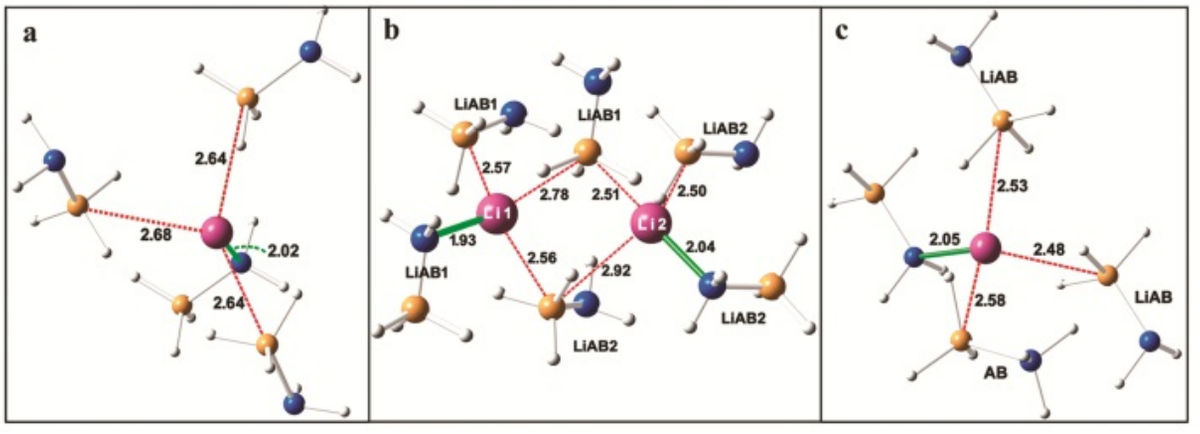

Figure 13. Coordination of Li^+ in (a) α-LiAB, (b) β-LiAB, and (c) LiAB·AB. Li: purple spheres; B: brown spheres; N: blue spheres; and H: white spheres. Reproduced from Ref. [53] with permission.

http://dx.doi.org/10.5772/61048

4.3. Potassium amidoborane (KNH_2BH_3, KAB)

Through the reaction of AB with an equivalent KH, polycrystalline KAB was synthesized in THF, while single crystal was obtained in a mixed solvent of diglyme and hexane at room temperature [40]. Similar to LiAB and NaAB, KAB crystallizes in an orthorhombic cell (space group *Pbca*) with lattice parameters of a = 9.4304(1) Å, b = 8.26112(1) Å, and c = 17.3403(2) Å. However, different from Li^+ in LiAB and Na^+ in NaAB, K^+ is octahedrally coordinated by $[NH_2BH_3]^-$ groups with the formation of three K-N bonds (3.0207-3.1345 Å) and three K···BH_3 coordinations (Figure 14A). The distance of closest NH···HB (2.265 Å) in KAB is smaller than those in LiAB (2.372 Å) and NaAB (2.717 Å). As shown in Figure 14B, an endothermic peak for melting was observed before an exothermic event for hydrogen release. It could release 1.5 Eq of H_2 (6.5 wt%) at ~80 °C. With the temperature increase to 160 °C, another 0.5 Eq of H_2 was released. No ammonia or borazine was detected throughout the dehydrogenation.

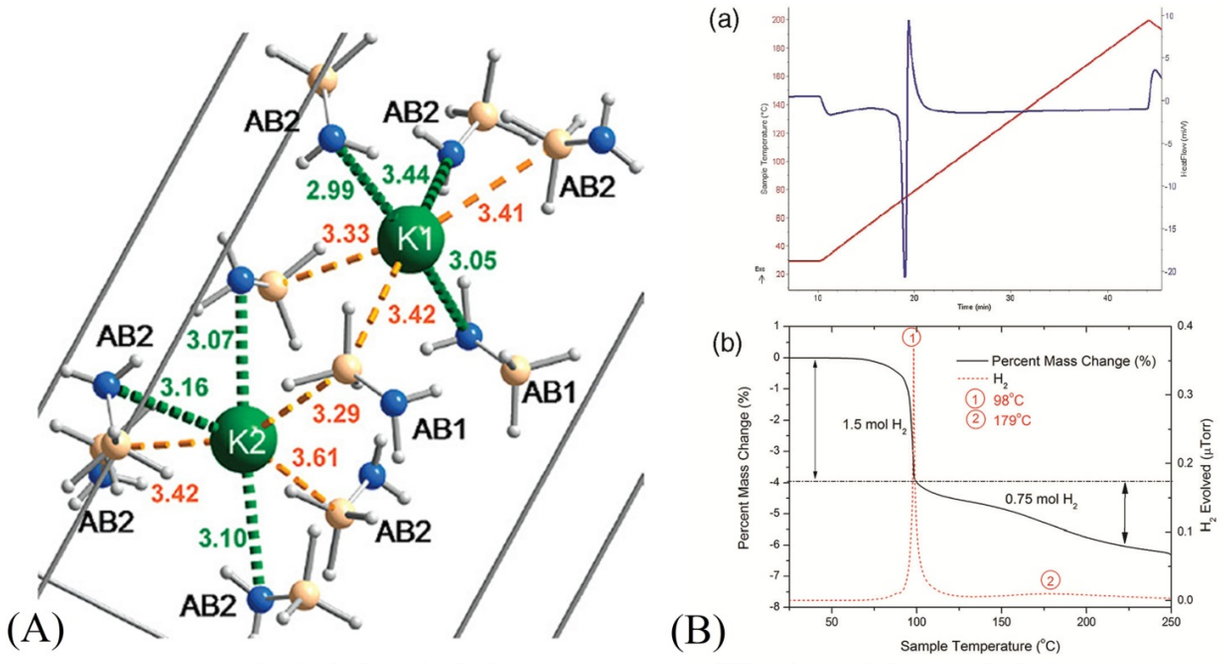

Figure 14. (A) Crystal structure of KAB. K: green spheres; N: blue spheres; B: cream spheres; and H: white spheres. (B) (a) DSC and (b) IGA data for KAB decomposition. Reproduced from Ref. [40] with permission.

4.4. Magnesium amidoborane ($Mg(NH_2BH_3)_2$, MgAB)

MgAB is supposed to be a promising material for storing hydrogen because it has a hydrogen content of 11.8 wt%. However, it is unsuccessful to prepare crystalline MgAB either by ball milling method or *via* wet-chemical method until the beginning of 2013. MgAB was synthesized through aging treatment of post-milled 2AB/MgH_2 or 2AB/Mg powder, in which the

formation of MgAB was not a straightforward process but experienced a prerequisite step of phase transition [55]. However, the crystal structure was failed to solve. In 2010, its structure was successfully proposed through theoretical simulation [15]. MgAB has a monoclinic cell (space group *C*2) with lattice parameters of a = 8.5772 Å, b = 5.6048 Å, c = 5.6216 Å, and β = 85.8476°. Two Mg-N bonds with the length of 2.111 Å and two Mg···BH_3 coordinations are around Mg^{2+} (Figure 15). As a stable compound at room temperature, MgAB could release ~10 wt% H_2 at 300 °C, without volatile by-products detectable [55].

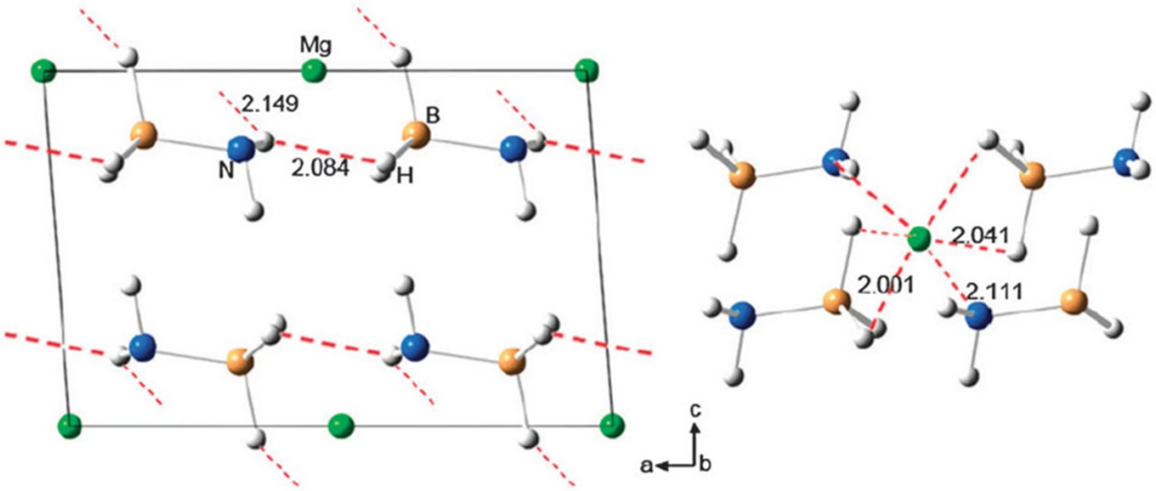

Figure 15. Simulated crystal structure of MgAB. Mg: green spheres; N: blue spheres; B: orange spheres; and H: white spheres. Reproduced from Ref. [15] with permission.

4.5. Calcium amidoborane ($Ca(NH_2BH_3)_2$, CaAB)

Due to the strong coordination between solvent and metal cation, CaAB·2THF adduct rather than pure CaAB was first synthesized through reacting CaH_2 with two equivalent AB in THF [39]. The specially octahedral coordination of Ca^{2+} with two NH_2, two BH_3, and two O resulted in an extended chain-like structure. After desiccation under a dynamic flow of argon, about 10% remaining THF was evolved from 70 °C to 105 °C, and hydrogen was released mainly from 120 to 245 °C. Another adduct of [(DIPP-nacnac)$CaNH_2BH_3(THF)_2$] was also reported [56], in which Ca^{2+} is octahedrally coordinated to DIPP-nacnac [(2,6-$iPr_2C_6H_3$)NC(Me)C(H)C(Me)N(2,6-$iPr_2C_6H_3$)] bidentate ligand, $[NH_2BH_3]^-$, THF. Using mechanical milling method from CaH_2 and two equivalent AB, Wu et al. [38] synthesized a solvent-free CaAB, which crystallizes in a monoclinic cell (space group *C*2) with lattice parameters of a = 9.100(2) Å, b = 4.371(1) Å, c = 6.441(2) Å, and β = 93.19°. Ca^{2+} is octahedrally coordinated through two Ca-N bonds with the length of ~2.466 Å and four coordinations of Ca···BH_3 with the distance in the range of 2.87-3.03 Å (Figure 16). Different from the CaAB

http://dx.doi.org/10.5772/61048

adducts, there are two steps for hydrogen release with peaks at 100 and 140 °C. Upon heating to 250 °C, 2 Eq of H_2 was released with the solid residues in amorphous state.

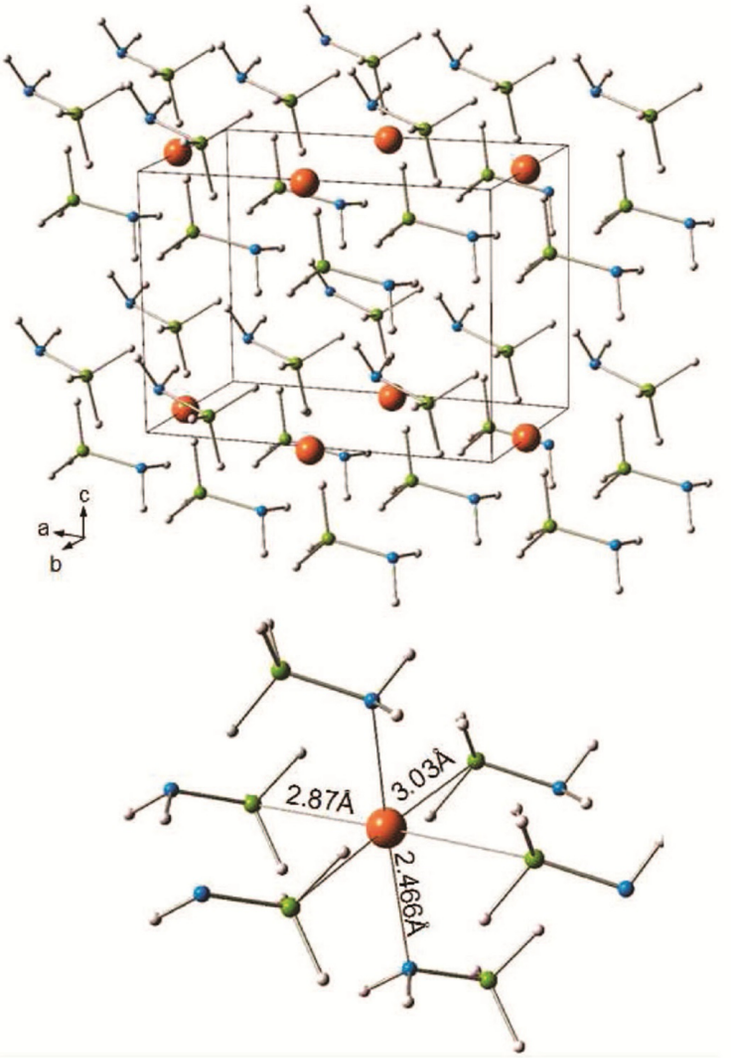

Figure 16. (Top) Crystal structure of CaAB. Ca: orange spheres; B: green spheres; N: blue spheres; and H: white spheres. (Bottom) Coordination environment of Ca^{2+}. Reproduced from Ref. [38] with permission.

4.6. Strontium amidoborane ($Sr(NH_2BH_3)_2$, SrAB)

Through reacting SrH_2 with AB in a 1:2 molar ratio, SrAB was successfully synthesized by moderate milling and the following heating treatment at 45 °C [41]. Similar to CaAB, SrAB also crystallizes in a monoclinic cell (space group *C*2) with lattice parameters of a = 8.1660(4) Å, b = 5.0969(3) Å, c = 6.7258(4) Å, and β = 94.392(4)°. Sr^{2+} is octahedrally coordinated by $[NH_2BH_3]^-$ groups to form two Sr-N bonds with a length of 2.68 Å and four Sr···BH_3 coordinations (Figure 17). Upon heating, SrAB started to decompose into H_2 and $Sr(NBH)_2$ at about 60 °C. In an isothermal dehydrogenation performed at a temperature of 80 °C, 4 Eq of H_2 could

be rapidly released in a few minutes. However, the evolved hydrogen was contaminated by undesirable by-products of NH_3 and B_2H_6 evolved from the decomposition of the resulting $Sr(NBH)_2$.

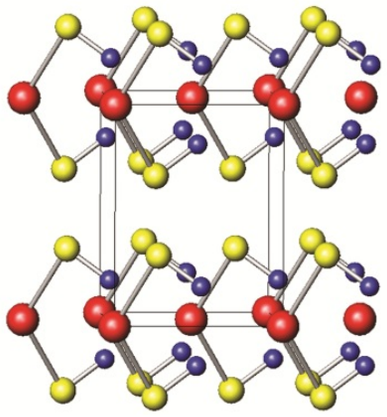

Figure 17. Crystal structure of SrAB. Sr: red spheres; N: yellow spheres; and B: blue spheres. Reproduced from Ref. [41] with permission.

4.7. Yttrium amidoborane ($Y(NH_2BH_3)_3$, YAB)

Ball milling YCl_3 with three equivalent LiAB gave rise to the formation of YAB [42]. In fact, it was a homogenous mixture with a side product of LiCl, which is very difficult to separate. YAB has a monoclinic cell (space group $C2/c$) with lattice parameters of a = 13.18902(63) Å, b = 7.82233(38) Å, c = 14.874274(68) Å, and β = 92.42620(40)°. However, it was thermodynamically unstable and spontaneously decomposed in several days at room temperature. A large amount of H_2 with NH_3 impurity was released from freshly prepared sample upon heating to 250 °C. Motivated by the synthesis of YAB, the attempt to synthesize iron (III) amidoborane ($Fe(NH_2BH_3)_3$, FeAB) through metathesis of $FeCl_3$ and three equivalent LiAB in THF was unsuccessful [57]. Instead of FeAB formation, 1.5 Eq of H_2 was released and a black solid containing LiCl was produced. Meanwhile, Fe^{3+} was reduced during dehydrogenation evidenced by Mössbauer and XAFS characterizations.

4.8. $Na[Li(NH_2BH_3)_2]$

$Na[Li(NH_2BH_3)_2]$ was reported to be the first mixed-cation amidoborane, which was prepared by milling a mixture of NaH/LiH/2AB performed on a high-energy disk mill [58]. It crystallizes in a triclinic cell (space group $P\bar{1}$) with lattice parameters of a = 5.0197(4) Å, b = 7.1203(7) Å, c = 8.9198(9) Å, α = 103.003(6)°, β = 102.200(5)°, and γ = 103.575(5)° [58]. As shown in Figure 18B, Na^+ is octahedrally coordinated with H atoms from BH_3 groups with different Na-H distances, while Li^+ is tetrahedrally coordinated by one H atom from BH_3 group and three N atoms from NH_2 groups. In addition, the formed chains of dimeric $[Li(NH_2BH_3)_2]_2^-$ anions linked through Li···H coordinations were found in $Na[Li(NH_2BH_3)_2]$. Thus, $Na[Li(NH_2BH_3)_2]$ was regarded as an ionic compound composed of Na^+ and $[Li(NH_2BH_3)_2]_2^-$, which is totally

http://dx.doi.org/10.5772/61048

different from NaAB and LiAB. $Na[Li(NH_2BH_3)_2]$ decomposed exothermally from 75 °C to 110 °C with 6.0 wt% H_2 released. An additional 3.0 wt% H_2 could be released in the temperature range of 110-200 °C. During its decomposition, there was an evolution of ammonia [58]. One year later, Li et al. [59] prepared $Na[Li(NH_2BH_3)_2]$ through a wet-chemical method, i.e., recrystallizing a mixture of LiAB/NaAB (1:1 molar ratio) or reacting AB with a post-milled mixture of LiH/NaH (1:1 molar ratio) in THF. However, $Na[Li(NH_2BH_3)_2]$ was theoretically determined to be in an orthorhombic cell (space group of $Pca2_1$) with lattice parameters of a = 14.639 Å, b = 7.169 Å, and c = 5.367 Å, which is significantly different from the structure determined experimentally. For example, the coordination environments of Li^+ and Na^+ are similar in its simulated structure, i.e., surrounded by one N atom from $[NH_2BH_3]^-$ and six H atoms from $[NH_2BH_3]^-$ (Figure 18A). Furthermore, the calculated free energy $\Delta G(x)$ indicated that all of the studied compositions in $Na_xLi_{1-x}NH_2BH_3$ except x = 0.125 were also thermodynamically favored [59].

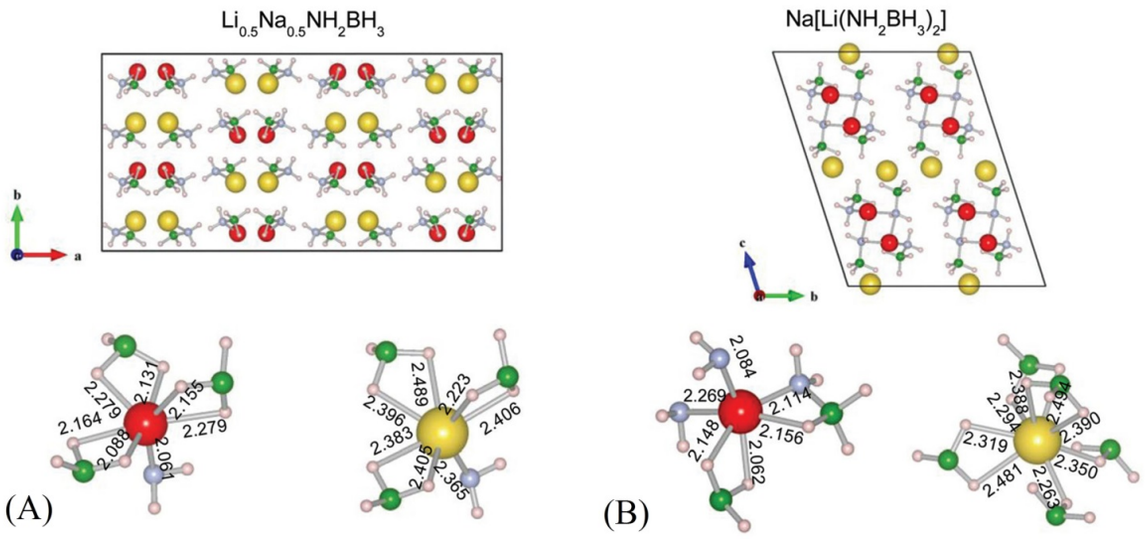

Figure 18. Crystal structure of $Na[Li(NH_2BH_3)_2]$ determined theoretically (A) and experimentally (B). Coordinations of Li^+ and Na^+ are displayed under each structure. Li: big red spheres; Na: big yellow spheres; N: small light blue spheres; B: small green spheres; and H: small pink spheres. Reproduced from Ref. [59] with permission.

4.9. $NaMg(NH_2BH_3)_3$

Almost at the same time, another dual-metal (alkali metal and alkaline-earth metal) amidoborane, namely, $NaMg(NH_2BH_3)_3$, was reported [60]. It was prepared by mechanically milling $3AB/NaMgH_3$ powdery mixture and the following treatment at 45 °C according to the reaction equation: $3NH_3BH_3 + NaMgH_3 \rightarrow NaMg(NH_2BH_3)_3 + 3H_2$. From its SR-XRD pattern, $NaMg(NH_2BH_3)_3$ was ascribed to a monoclinic cell (space group $P2_1$ or $P2_1/m$) with lattice parameters of a = 17.011 Å, b = 9.432 Å, c = 9.398 Å, and β = 115.99°. However, the detailed crystal structure was unsuccessfully solved in reference [60]. For the post-milled $3AB/NaMgH_3$ without heating treatment, there were two steps for dehydrogenation. It started to release H_2 exothermically at around 50 °C for the first step with yielding about 3.5 wt% H_2,

which agrees well with the amount of hydrogen released during heating treatment at 45 °C. Therefore, it could be concluded that the first step for dehydrogenation gave rise to the formation of $NaMg(NH_2BH_3)_3$ and the second one was for its own dehydrogenation with the beginning at about 140 °C and the most rapid release rate at about 170 °C. No volatile by-products and sample foaming were observed during the decomposition process upon heating to 250 °C. It is worth noting that the dehydrogenation was determined to be of mild endothermicity of 3.4 kJ (mol H_2)$^{-1}$, which is the first case reported so far and entirely different from the exothermic dehydrogenation for monometal amidoboranes of NaAB and MgAB. This indicates that dual-cation combination in amidoboranes plays a vital role in altering their dehydrogenation thermodynamics. From thermodynamic point of view, the endothermic dehydrogenation provides a possibility to achieve rehydrogenation at moderate conditions. However, in this study, it was unsuccessful to recharge the solid residual at moderate conditions.

4.10. $Na_2Mg(NH_2BH_3)_4$

$Na_2Mg(NH_2BH_3)_4$ was first synthesized by ball milling a mixture of NaH/MgH_2/2AB [61]. It was identified to have a space group of $I4_1/a$ and approximate lattice parameters of a = 9.415 Å and c = 12.413 Å. The crystal structure illustrated in Figure 19 shows that Mg^{2+} is coordinated with four $[NH_2BH_3]^-$ groups *via* Mg-N bonds (2.104 Å) to form $[Mg(NH_2BH_3)_4]^{2-}$ tetrahedron. Na^+ is octahedrally coordinated only with six BH_3 groups with the distances of Na-B ranging from 2.900 to 3.634 Å. The distances of Na-H coordinations between Na^+ and its close hydridic H in BH_3 groups are in the range of 2.383-2.943 Å. As a consequence, Mg^{2+} and Na^+ are linked through different coordinations with both ends of the bridging $[NH_2BH_3]^-$ groups and form an ordered structure in coordinations. $Na_2Mg(NH_2BH_3)_4$ had an onset temperature for dehydrogenation at ~65 °C and a total amount of 8.4 wt% H_2 was released upon heating to 200 °C, with contamination by trace amount of borazine and ammonia. In another paper [62], a wet-chemical method was proposed to synthesize pure $Na_2Mg(NH_2BH_3)_4$. Typically, a solid mixture of $Mg(NH_2)_2$/2NaH/4AB was introduced into THF. After 0.7 Eq of gaseous products (H_2 and NH_3) was released, pure $Na_2Mg(NH_2BH_3)_4$ as the precipitate was obtained through filtration, which agrees well with the one synthesized by ball milling method [61].

4.11. $K_2Mg(NH_2BH_3)_4$

$K_2Mg(NH_2BH_3)_4$ was synthesized by ball milling method according to the reaction equation: $2Mg(NH_2BH_3)\cdot NH_3 + 2KH \rightarrow K_2Mg(NH_2BH_3)_4 + Mg(NH_2)_2 + 2H_2$ [62]. Similarly, $Na_2Mg(NH_2BH_3)_4$ could also be prepared through this procedure. However, as a by-product, $Mg(NH_2)_2$ is very difficult to separate or remove. $K_2Mg(NH_2BH_3)_4$ crystallizes in a tetragonal cell (space group $I4_1/a$) with lattice parameters of $a = b$ = 9.5974(17) Å and c = 13.581(4) Å. As shown in Figure 20, Mg^{2+} is tetrahedrally coordinated with four N atoms (2.115 Å for Mg–N bond length) from four $[NH_2BH_3]^-$ groups to form $[Mg(NH_2BH_3)_4]^{2-}$ species. Unlike Mg^{2+}, without the formation of K–N bond, K^+ is octahedrally coordinated by six $[Mg(NH_2BH_3)_4]^{2-}$ groups through six K···BH_3 coordinations with K-B distances ranging from 3.361 to 3.617 Å. Due to the difficulties in the removal of $Mg(NH_2)_2$ from the products, the dehydrogenation

http://dx.doi.org/10.5772/61048

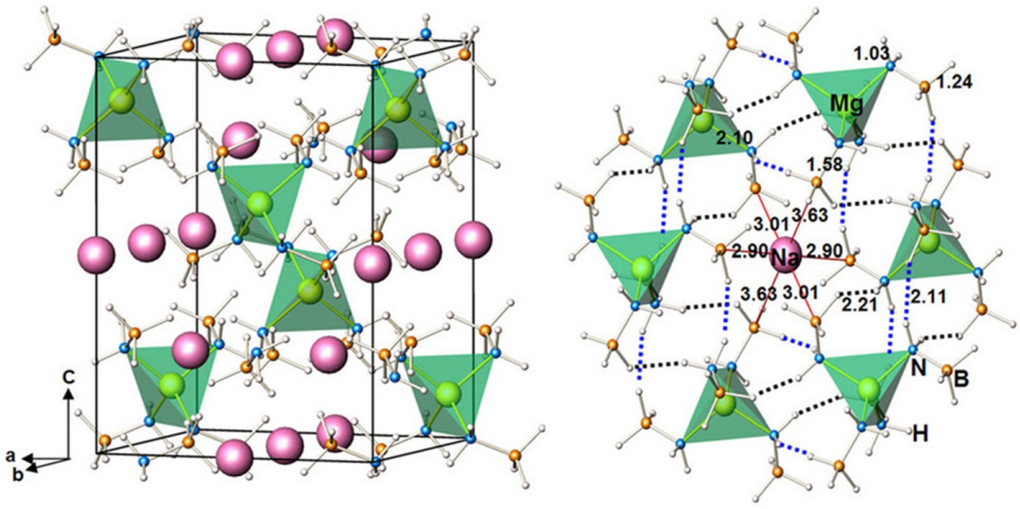

Figure 19. Crystal structure of $Na_2Mg(NH_2BH_3)_4$. Na: pink spheres; Mg: yellow spheres; N: blue spheres; B: orange spheres; and H: white spheres. Reproduced from Ref. [61] with permission.

was measured based on the composite of [$M_2Mg(NH_2BH_3)_4$ + $Mg(NH_2)_2$, (M = Na, K)] [62]. A very small amount of NH_3 was released from room temperature to 150 °C before dehydrogenation for both composites, with a mass loss of 3.7 and 3.8 wt%. Hydrogen was released with the most rapid rate at about 158 and 153 °C for [$K_2Mg(NH_2BH_3)_4$+$Mg(NH_2)_2$] and [$Na_2Mg(NH_2BH_3)_4$+$Mg(NH_2)_2$] composites, respectively. Most important of all, both composites exhibited the endothermic dehydrogenation in open system, i.e., 5.2 kJ (mol H_2)$^{-1}$ for [$Na_2Mg(NH_2BH_3)_4$+$Mg(NH_2)_2$] and 7.0 kJ (mol H_2)$^{-1}$ for [$K_2Mg(NH_2BH_3)_4$+$Mg(NH_2)_2$]. A total amount of about 7 and 7.8 wt% H_2 was achieved upon heating to 285 °C for these two composites. However, the role of $Mg(NH_2)_2$ remains unknown in inducing endothermic dehydrogenation of composites. Further research into the interaction between amide and dual-metal amidoborane is needed.

4.12. (Li,Al) amidoborane

Bimetallic (Li,Al) amidoborane was prepared by ball milling of 4AB/Li_3AlH_6 mixture [63]. It was also observed after heating a post-milled mixture of $LiAlH_4$/AB at 170 °C [64]. The information of crystal structure was not reported in both references [63,64]. It could release about 10 wt% H_2 at 200 °C, with a significant suppression of volatile by-products. The post-dehydrogenated products of (Li,Al) amidoborane could be regenerated through reduction by hydrazine in liquid ammonia. Around 3.5 wt% H_2 was released upon heating to 400 °C, corresponding to a 35% regeneration yield [63].

5. Metal amidoborane ammoniates

Ammonia was a hydrogen-rich compound (17.7 wt%). As a strong Lewis base, it is used as a ligand to form amine complexes with various compounds for hydrogen storage [65-69]. It is

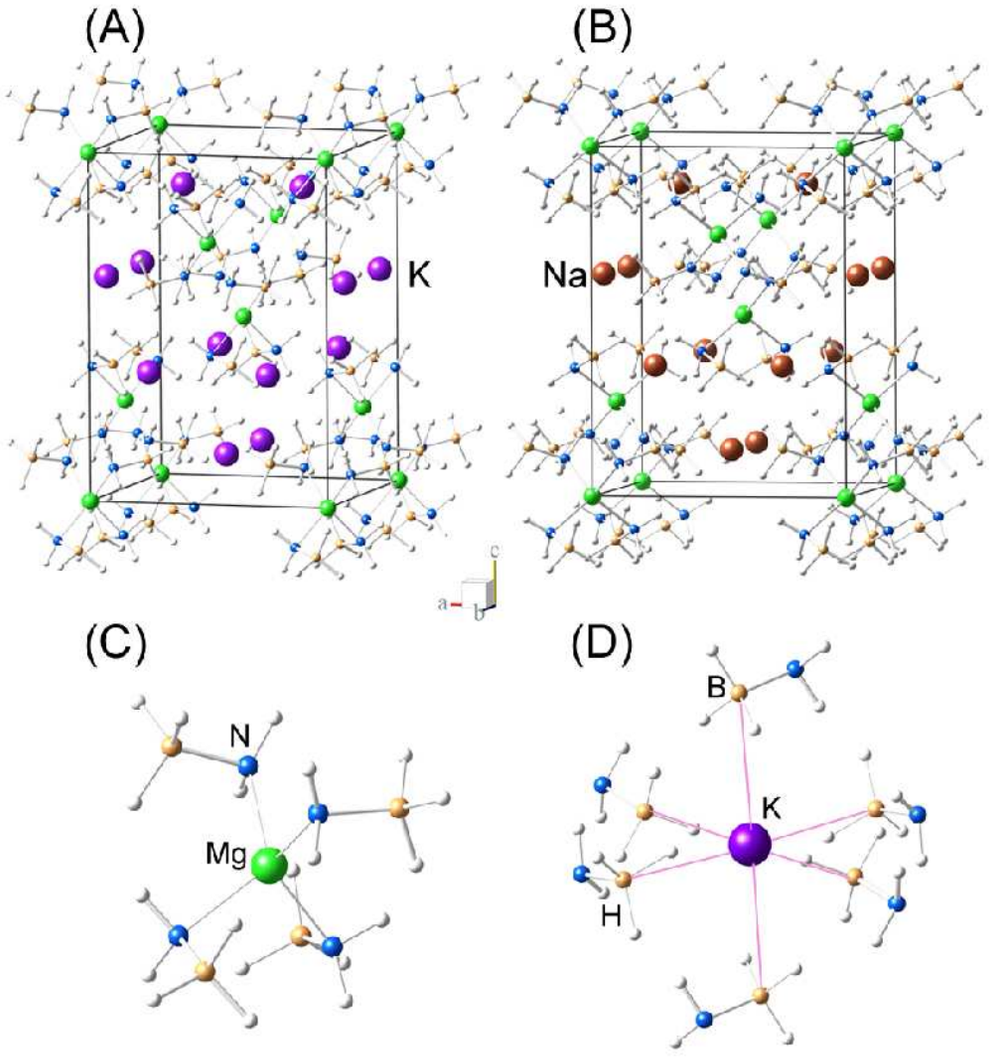

Figure 20. Crystal structure of (a) $K_2Mg(NH_2BH_3)_4$, (b) $Na_2Mg(NH_2BH_3)_4$, (c) Coordination of Mg^{2+}, and (d) Coordination of K^+. Reproduced from Ref. [62] with permission.

noted that because of the difference in electronegativity, positively charged H in NH_3 can interact with protic H in metal amidoboranes and borohydrides for facilitating hydrogen release.

5.1. Lithium amidoborane ammoniate ($LiNH_2BH_3 \cdot NH_3$, $LiAB \cdot NH_3$)

A new hybrid material with the formula of $LiNH_2BH_3NH_3$ was produced from the mixed AB and $LiNH_2$ in a 1:1 molar ratio, which can be treated as a monoammoniate of LiAB. It rapidly released 11.9 wt% H_2 under 250 °C, with the most rapid rate observed at 60 °C [70]. In fact, $LiAB \cdot NH_3$ was synthesized by reacting LiAB with an equivalent NH_3 [71]. At room temperature, it is a sticky matter in an amorphous state. Upon cooling to −20 °C, $LiAB \cdot NH_3$ becomes a solid and crystallizes in an orthorhombic cell (space group *Pbca*), which has the lattice parameters of $a = 9.711(4)$ Å, $b = 8.7027(5)$ Å, and $c = 7.1999(1)$ Å. However, the crystal structure

http://dx.doi.org/10.5772/61048

was not reported in reference [71]. At room temperature, $LiAB \cdot NH_3$ decomposed into ammonia and LiAB under vacuum. However, at temperatures more than 40 °C, favorable dehydrogenation was observed. Volumetric release test showed that about 6.2 wt% H_2 could be released at 70 °C under argon, while 11.2 wt% H_2 at 60 °C under ammonia.

5.2. Calcium amidoborane diammoniate ($Ca(NH_2BH_3)_2 \cdot 2NH_3$, $CaAB \cdot 2NH_3$)

In 2009, Chua et al. [72] reported the synthesis, structure, and dehydrogenation of $CaAB \cdot 2NH_3$. They provided two synthesizing methods, i.e., ball milling of $Ca(NH_2)_2/2AB$ mixture and reacting CaAB with two equivalent NH_3. It crystallizes in an orthorhombic cell (space group *Pna*21) with lattice parameters of $a = 18.673(3)$ Å, $b = 5.2283(8)$ Å, and $c = 8.5748(12)$ Å. Figure 21 shows that each Ca^{2+} has octahedral coordination through two $Ca \cdots NH_3$ coordinations (2.517 and 2.521 Å), two $Ca \cdots BH_3$ coordinations (2.650 and 2.807 Å), and two Ca-N bonds (2.397 and 2.521 Å), which results in a bonding network of $NH \cdots HB$ dihydrogen due to NH_3 coordinations. $CaAB \cdot 2NH_3$ decomposed into CaAB and 2 Eq of NH_3 under 100 °C in an open system. On the contrary, in a closed reactor, H_2 rather than NH_3 was released predominantly due to the existence of NH_3 equilibrium pressure, with an onset temperature at ~70 °C. Almost 9 wt% H_2 could be released upon heating to 300 °C. Compared to CaAB, the onset temperature has a 50 °C reduction and the dehydrogenation capacity at 300 °C has a 2 wt% increase.

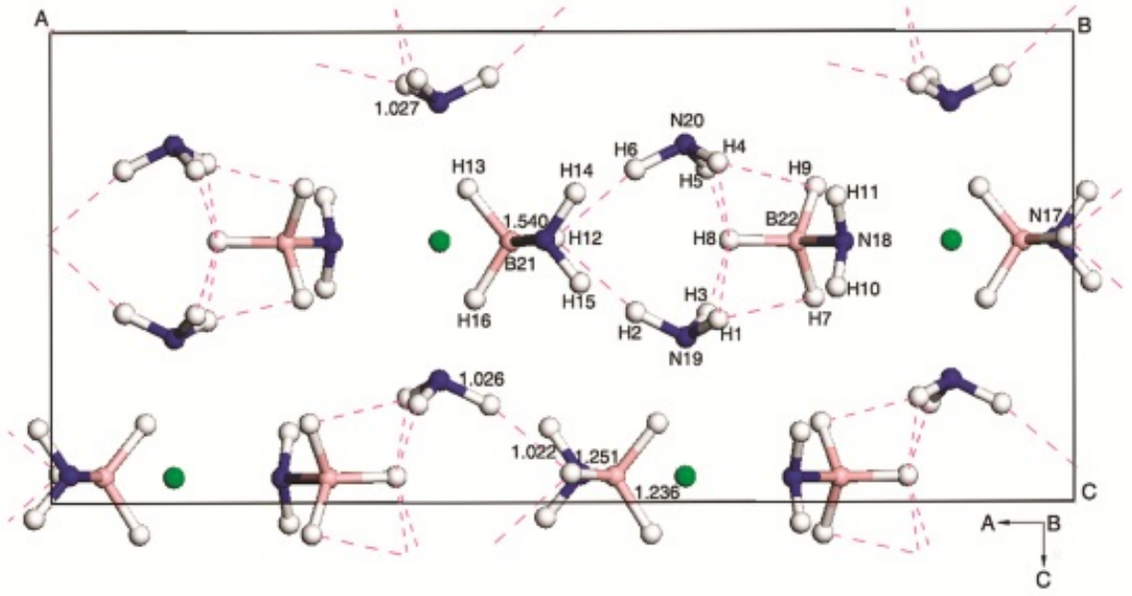

Figure 21. Crystal structure of $CaAB \cdot 2NH_3$. Ca: green spheres; N: blue spheres; B: pink spheres; and H: white spheres. Reproduced from Ref. [72] with permission.

5.3. Calcium amidoborane monoammoniate ($Ca(NH_2BH_3)_2 \cdot NH_3$, $CaAB \cdot NH_3$)

$CaAB \cdot NH_3$ was prepared by ball milling a mixture of CaNH/2AB [73]. Alternatively, ball milling a mixture of $Ca(NH_2)_2/CaH_2/4AB$ could also give rise to the formation of $CaAB \cdot NH_3$

with accompanying 2 Eq of H_2 released. It crystallizes in a monoclinic cell (space group of $P2_1/c$) with lattice parameters of a = 10.5831(14) Å, b = 7.3689(11) Å, c = 10.2011(13) Å, and β = 120.796(6)° [73]. Unlike CaAB·2NH_3, Ca^{2+} in CaAB·NH_3 has a geometry of trigonal bipyramid (Figure 22), in which Ca^{2+} is surrounded by two NH_2 from $[NH_2BH_3]^-$ groups through Ca-N bonds (2.400 and 2.465 Å), two BH_3 from $[NH_2BH_3]^-$ groups through Ca···BH_3 interactions (2.669-3.182 Å), and one NH_3 through Ca···NH_3 interaction (2.472 Å). The special structure resulted in the network of NH···HB dihydrogen bond. TG-DSC-MS tests revealed that NH_3 was predominantly released under 100 °C with a weight loss of 12.6%, while 6.2 wt% H_2 was solely released from 100 to 300 °C. Compared with the theoretical value for deammoniation of CaAB·NH_3 (~14.5 wt%) and for dehydrogenation of CaAB (~8 wt%), some NH_3 should participate in dehydrogenation under 100 °C, which is evidenced by the concurrent release of H_2 from MS. However, in a closed reactor, hydrogen release in two steps was observed with an exothermic event detected in the first step. At 300 °C, 6 Eq of H_2 (~10.2 wt%) could be released, in which the amount of by-product NH_3 is less than 0.1 Eq.

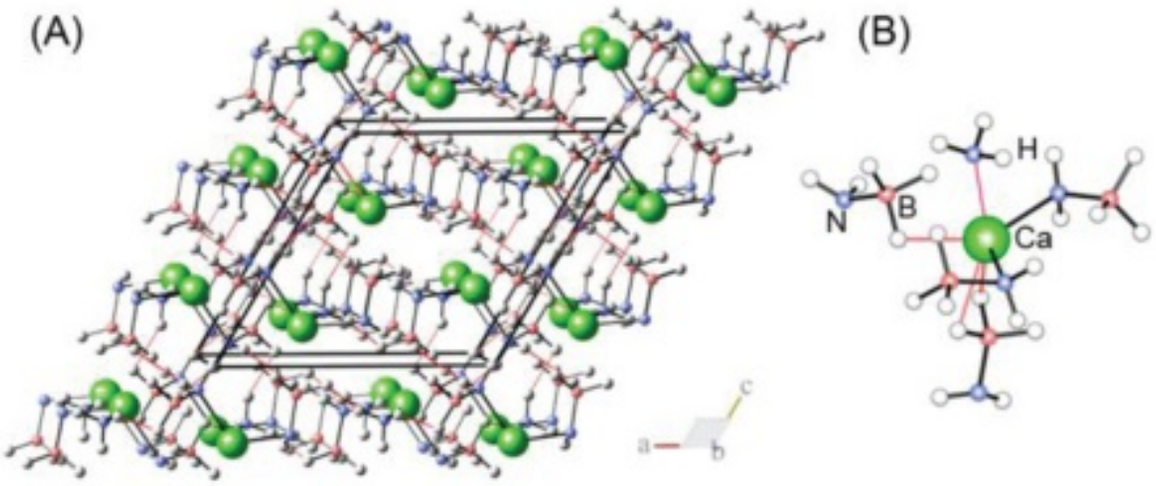

Figure 22. A) Crystal structure of CaAB·NH_3. (B) Coordination of Ca^{2+}. Ca: green spheres; N: blue spheres; B: pink spheres; and H: white spheres. Reproduced from Ref. [73] with permission.

5.4. Magnesium amidoborane monoammoniate ($Mg(NH_2BH_3)_2 \cdot NH_3$, MgAB·$NH_3$)

Ball milling a mixture of $Mg(NH_2)_2$/2AB could give rise to the formation of magnesium amidoborane diammoniate ($Mg(NH_2BH_3)_2 \cdot 2NH_3$, MgAB·2$NH_3$). Unlike solid CaAB·2$NH_3$, MgAB·2$NH_3$ is a liquid matter at ambient condition. Upon releasing 1 Eq of NH_3, solid MgAB·NH_3 was formed [74]. Alternatively, MgAB·NH_3 could also be prepared by ball milling a mixture of MgNH/2AB [74]. In a monoclinic cell (space group of $P21/a$), MgAB·NH_3 has the lattice parameters of a = 8.8815(6) Å, b = 8.9466(6) Å, c = 8.0701(5) Å, and β = 94.0744(48)°. As shown in Figure 23, each Mg^{2+} has a tetrahedral coordination, in which Mg^{2+} forms two Mg-N bonds (2.104 and 2.129 Å) with the adjacent $[NH_2BH_3]^-$ groups, a Mg···NH_3 coordination (2.157 Å) with the adjacent NH_3, and a Mg···BH_3 coordination (2.126 Å) with the adjacent

http://dx.doi.org/10.5772/61048

$[NH_2BH_3]^-$ group. In $MgAB \cdot NH_3$, a dihydrogen bonding network was established through the interactions of NH···HB between NH_3 and BH_3 groups. Different from $CaAB \cdot 2NH_3$ and $CaAB \cdot NH_3$, the decomposition of $MgAB \cdot NH_3$ in an open system exhibited direct desorption of H_2 instead of NH_3, indicating easier interaction between $H^{\delta+}$ in NH_3 and $H^{\delta-}$ in BH_3 to the formation of H_2 or stronger Mg···NH_3 coordination. Hydrogen release of $MgAB \cdot NH_3$ started at about 50 °C, with 5.7 Eq of H_2 (11.4 wt%) released up to 300 °C. An amorphous solid residue with chemical composition of MgB_2N_3H was left. NH_3 was undetectable during the whole dehydrogenation process, which evidenced the complete conversion of NH_3.

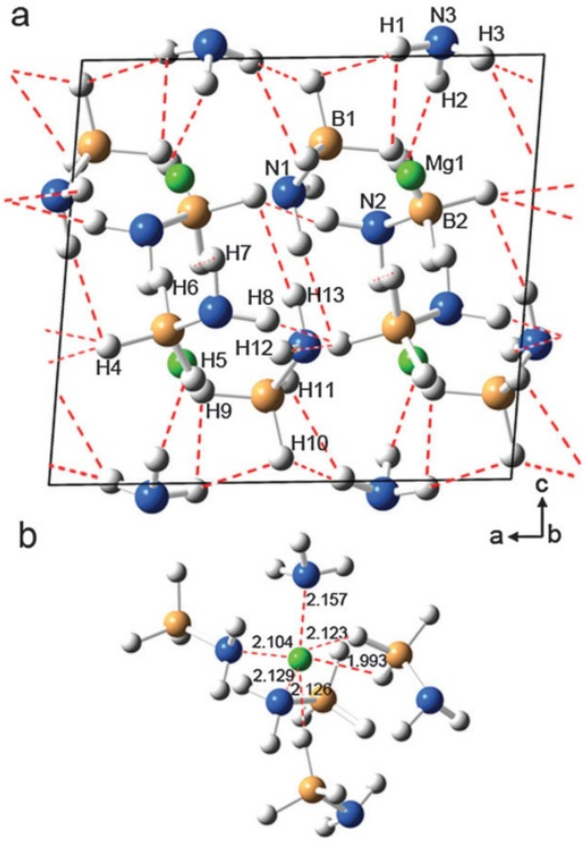

Figure 23. (a) Crystal structure of $MgAB \cdot NH_3$, and (b) Coordination of Mg^{2+}. Mg: green spheres; N: blue spheres; B: orange spheres; and H: white spheres. Reproduced from Ref. [74] with permission.

6. Metal borohydride-ammonia borane complexes

6.1. $2LiBH_4 \cdot NH_3BH_3$, $2LiBH_4 \cdot AB$

In 2010, the first metal borohydride-ammonia borane complex, namely, $2LiBH_4 \cdot AB$, was reported [75]. It was synthesized by ball milling AB with two equivalent $LiBH_4$ and had an orthorhombic structure (space group *Pnma*) with lattice parameters of a = 8.3118(8) Å, b = 12.428(1) Å, and c = 6.5944(7) Å. Figure 24 shows that there are alternating layers of borohydride

and AB in $2LiBH_4 \cdot AB$. And Li^+ and BH_4^- in the layer of borohydride remain their original configuration in pristine $LiBH_4$. Li^+ has a tetrahedral coordination with one AB and three BH_4^- groups. The distances between Li and H in BH_4^- are in the range of 2.023-2.246 Å, analogous to those between Li and its two close hydridic H in AB (2.078 and 2.321 Å). The BH···HN distances between BH_4^- and its nearby AB range from 2.248 to 2.254 Å, whereas the BH···HN distance between the adjacent AB is 2.439 Å. Such a weak BH···HN interaction in AB layers may be ascribed to the reinforced interactions of AB with the nearby H in BH_4^- and also with Li^+. Consequently, the intercalation of AB molecules into the crystal structure of $LiBH_4$ is basically stabilized by the interactions of AB with Li^+ and BH_4^-. There were two steps for dehydrogenation of $2LiBH_4 \cdot AB$, i.e., the first step occurring at 105-135 °C and the second one at 360 °C, which are determined to be the dehydrogenation of pristine AB and $LiBH_4$, respectively. In addition, the suppression of ammonia was achieved compared with pristine AB. It is worth noting that the dehydrogenated products of $2LiBH_4 \cdot AB$ could reabsorb 2.4 wt % H_2 at 400 °C under 82 bar H_2 pressure. In contrast, MBH_4-AB (M = Na, K) do not form new compounds during mechanochemical treatment [76].

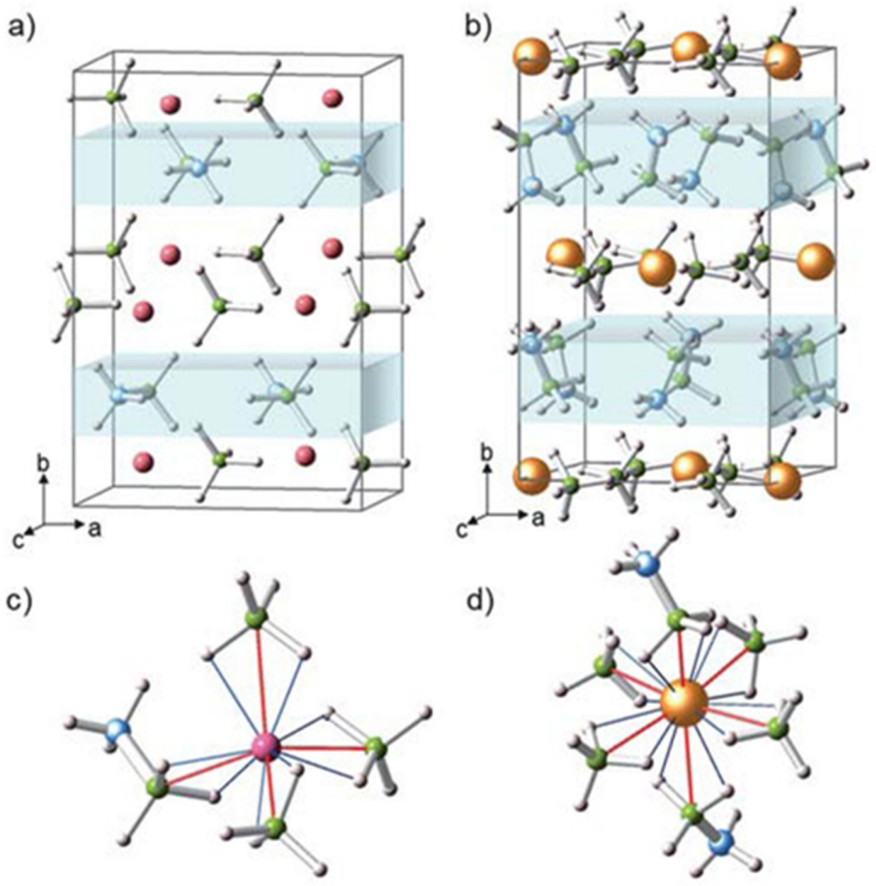

Figure 24. Crystal structure of (a) $2LiBH_4 \cdot AB$ and (b) $Ca(BH_4)_2 \cdot AB$. Coordination of (c) Li^+ and (d) Ca^{2+}. Li: pink spheres; Ca: orange spheres; B: green spheres; N: blue spheres; and H: white spheres. Reproduced from Ref. [75] with permission.

http://dx.doi.org/10.5772/61048

6.2. $LiBH_4 \cdot NH_3BH_3$, $LiBH_4 \cdot AB$

$LiBH_4 \cdot AB$ was prepared by mechanically milling AB with an equivalent $LiBH_4$ [77]. It crystallizes in a monoclinic cell (space group $P2_1$) with lattice parameters of a = 14.3131 (11) Å, b= 4.3634 (5) Å, c= 15.3500(13) Å, and β= 90.325(11)°. In $LiBH_4 \cdot AB$, there are $LiBH_4$ columns running along the b axis (Figure 25), which is notably different from $2LiBH_4 \cdot AB$. $LiBH_4$ columns are segregated by the adjacent AB molecules and thus lose the structural similarity to pristine one. In such an arrangement, Li^+ has two different coordination environments, both of which have a trigonal-planar coordination. One is coordinated by two BH_4^- and AB groups and the other by three BH_4^- groups. The unique coordination of Li^+ results in the remarkable variations of the interactions of Li^+ with its adjacent anions. For example, the distances of Li–B are ranging from 2.22 to 2.81 Å. While the distances between Li and its two close hydridic H in AB are 1.78 and 2.07 Å, much smaller than those in $2LiBH_4 \cdot AB$ (2.08 and 2.32 Å) [75], which indicates a stronger interaction between AB and Li^+. The BH···HN distances between AB and the adjacent BH_4^- are in a range of 1.85–2.31 Å, and those between nearby AB in AB layers are 1.86–2.39 Å, which demonstrates the presence of strong dihydrogen bonding throughout $LiBH_4 \cdot AB$. For thermolysis, $LiBH_4 \cdot AB$ first decomposed into $2LiBH_4 \cdot AB$ and AB at about 54 °C and then exhibited a three-step dehydrogenation, with release of a total amount of ~15.7 wt % H_2 upon heating to 450 °C. Interestingly, *h*-BN was found to form in the post-dehydrogenated product at a moderate temperature of 450 °C (compared with other methods for *h*-BN preparation), which resulted in the improved rehydrogenation and the following dehydrogenation properties of $LiBH_4 \cdot AB$ sample.

6.3. $Ca(BH_4)_2 \cdot NH_3BH_3$, $Ca(BH_4)_2 \cdot AB$

$Ca(BH_4)_2 \cdot AB$ was prepared by ball milling $Ca(BH_4)_2$ with an equivalent of AB, which had an orthorhombic cell (space group *Aba*2) with lattice parameters of a = 8.265(1) Å, b = 13.478(2) Å, and c = 8.136(1) Å [75]. Each Ca^{2+} has an octahedral coordination, surrounded by two AB molecules with Ca–B distances ranging from 2.899 to 2.923 Å and four BH_4^- groups (Figure 24). Unlike $2LiBH_4 \cdot AB$, the BH···HN distance between neighboring AB in AB layers of $Ca(BH_4)_2 \cdot AB$ is 1.735 Å, which indicates more powerful dihydrogen bonding. Through dihydrogen bonding, AB also interacts with its adjacent BH_4^- with the BH···HN distances of 1.986–2.037 Å. Furthermore, the distances between Ca^{2+} and its two close hydridic H of AB are 2.441 and 2.504 Å, similar to those between Ca^{2+} and H in BH_4^- (2.412–2.477 Å). As a consequence, different from $2LiBH_4 \cdot AB$, AB layers and $Ca(BH_4)_2$ layers are interlaced primarily by dihydrogen bonding in $Ca(BH_4)_2 \cdot AB$. For the case of hydrogen release, it has similar dehydrogenation behaviors with $2LiBH_4 \cdot AB$, i.e., independent dehydrogenation of AB and $Ca(BH_4)_2$ was observed, although the dehydrogenation temperature was slightly reduced to some extent.

6.4. $Mg(BH_4)_2 \cdot 2NH_3BH_3$, $Mg(BH_4)_2 \cdot 2AB$

$Mg(BH_4)_2 \cdot 2AB$ was prepared by ball milling $Mg(BH_4)_2$ with 2 equivalent AB [78,79]. It has an orthorhombic unit cell (space group $P2_12_12_1$) with lattice parameters of a = 14.4135(2) Å, b = 13.2084(2) Å, and c = 5.1118(1) Å. As shown in Figure 26, each Mg^{2+} has a tetrahedral coordi-

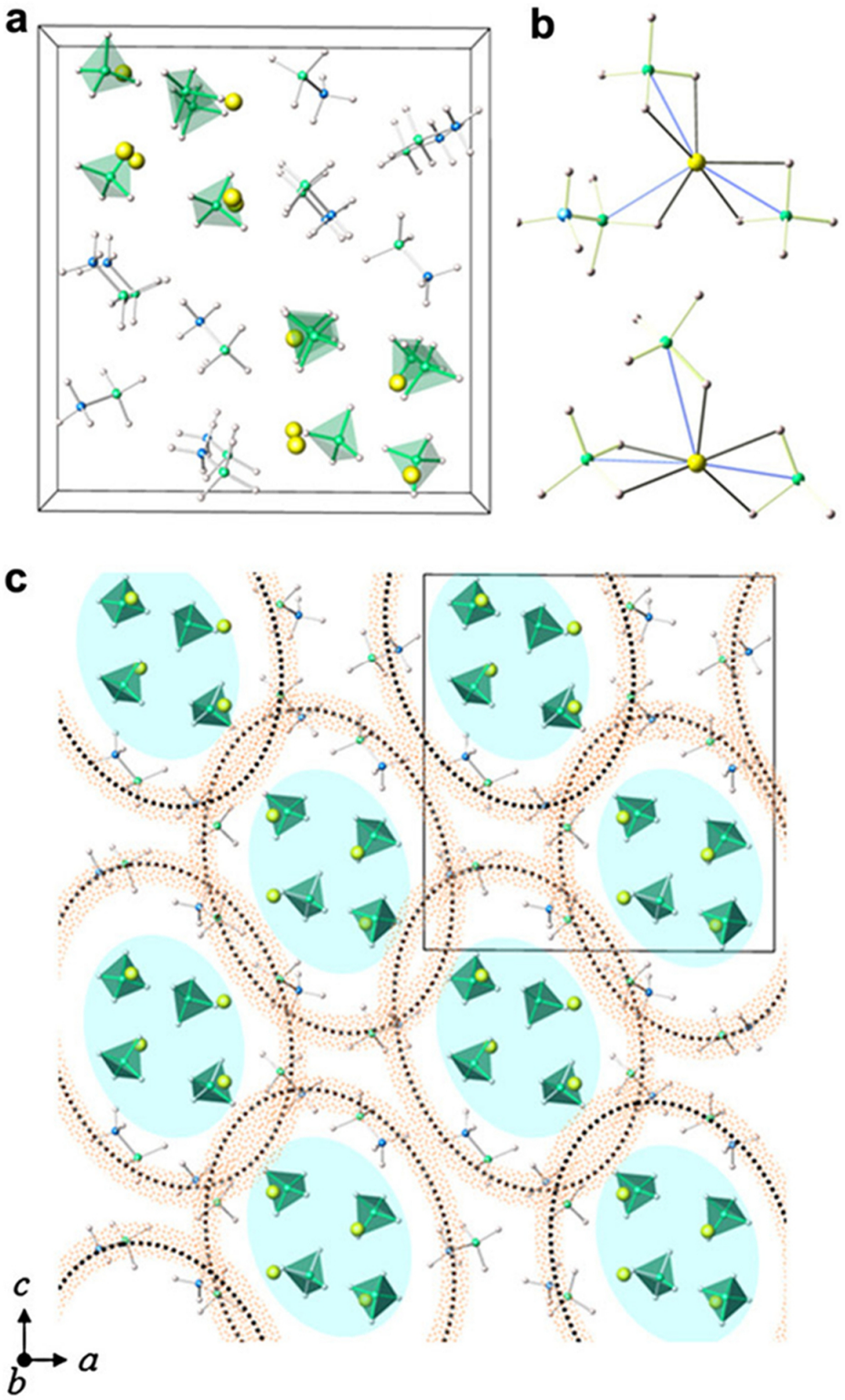

Figure 25. (a) Crystal structure of $LiBH_4 \cdot AB$. (b) Li^+ coordination. (c) Schematic arrangement of $LiBH_4$ and AB components in the crystal structure. Li: yellow spheres; B: green spheres; N: blue spheres; and H: white spheres. Reproduced from Ref. [77] with permission.

http://dx.doi.org/10.5772/61048

nation, surrounded by two BH_4^- groups and two AB groups with Mg-B distances in the range of 2.394–2.500 Å. The distances between Mg^{2+} and its close H in AB range from 2.062 to 2.106 Å, while the distances between Mg^{2+} and its close H in BH_4^- are in the range of 1.987-2.033 Å. Between AB and its nearby BH_4^- groups, there are BH···HN dihydrogen bonds with the distances in the range of 2.210-2.274 Å. $Mg(BH_4)_2 \cdot 2AB$ melted at 48 °C and started to release H_2 at 75 °C [79]. It had a broad dehydrogenation peak at 126 °C with a releasing trace amount of NH_3, B_2H_6, and borazine. The following dehydrogenation in the range of 200-400 °C was observed with two peaks at 297 °C and 340 °C. Volumetric release tests implied that the dehydrogenation behaviors of $Mg(BH_4)_2 \cdot 2AB$ look like a combination of pristine AB in 30-200 °C and $Mg(BH_4)_2$ in 200-400 °C.

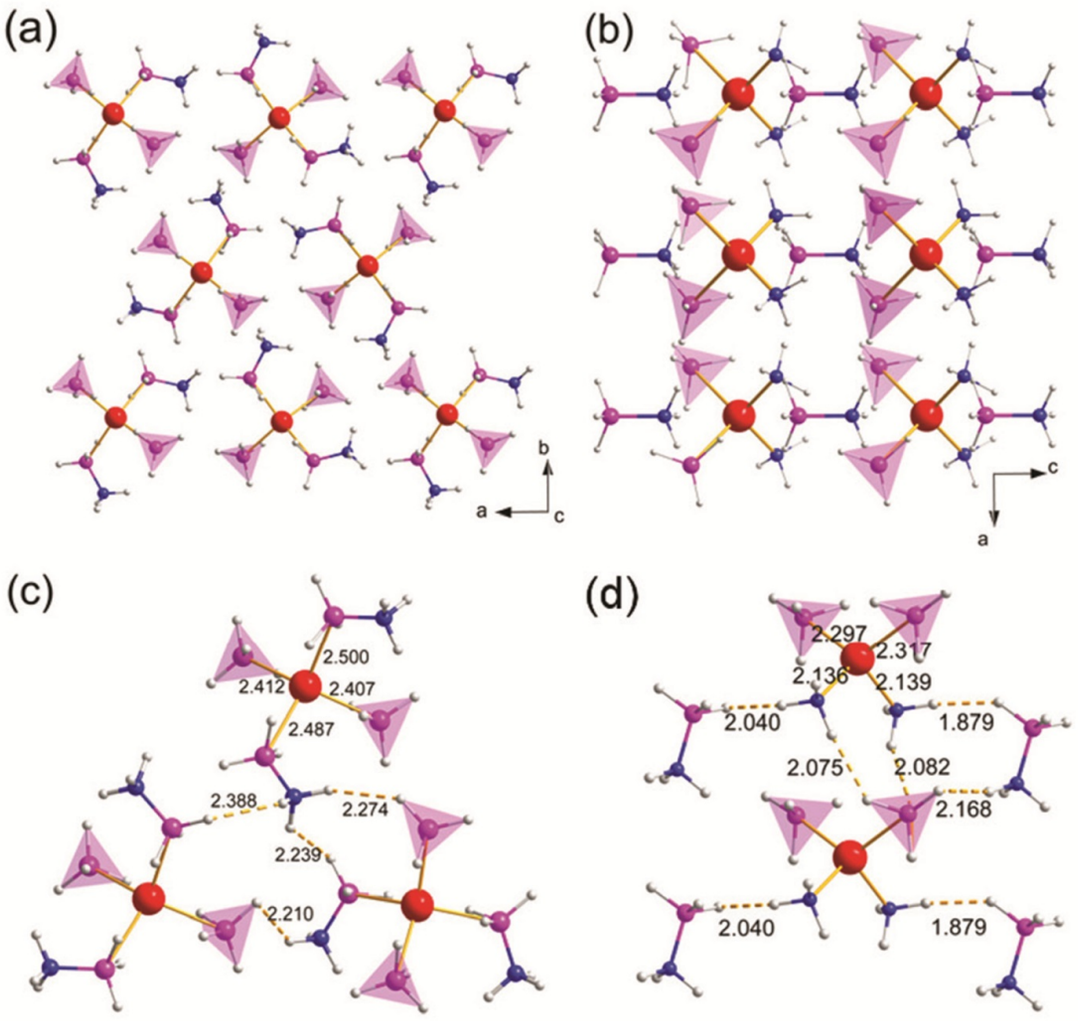

Figure 26. Crystal structure of (a) $Mg(BH_4)_2 \cdot 2AB$ and (b) $Mg(BH_4)_2 \cdot 2NH_3 \cdot AB$. Coordination of Mg^{2+} in (c) $Mg(BH_4)_2 \cdot 2AB$ and (d) $Mg(BH_4)_2 \cdot 2NH_3 \cdot AB$. Mg: red spheres; B: pink spheres; N: blue spheres; and H: white spheres. Reproduced from Ref. [78] with permission.

6.5. $Al(BH_4)_3 \cdot NH_3BH_3$, $Al(BH_4)_3 \cdot AB$

$Al(BH_4)_3 \cdot AB$ was synthesized through a reaction between $Al(BH_4)_3$ and an equivalent AB in a closed reactor at room temperature for 3 days, which could be accelerated by ball milling [80]. The resulting white crystals of $Al(BH_4)_3 \cdot AB$ revealed two polymorphs: the low-temperature α-phase and the high-temperature β-phase. Pure α-phase was found only in fresh samples, and it slowly transformed to β-phase at room temperature. Pure β-phase was obtained upon heating α-phase to about 62 °C with 1 °C min^{-1}, and it could not transform back to α-phase even cooling to -173 °C. Both phases crystallize in monoclinic cells with space group of $P2_1/c$ and Cc for α- and β-phase, respectively. α-phase has the lattice parameters of a = 7.8585(2) Å, b = 6.86473(14) Å, c = 15.7136(8) Å, and β = 96.429(4)°, while β-phase of a = 10.8196(8) Å, b = 7.2809(4) Å, c = 11.3260(9) Å, and β = 107.695(8)°. The crystal structures of $Al(BH_4)_3 \cdot AB$ in α-phase and β-phase are shown in Figure 27. In both structures, Al^{3+} is coordinated with one AB and three BH_4^- to form a distorted tetrahedron of AlB4. The interactions of NH···HB between NH_3 and BH_4^- groups were formed in $Al(BH_4)_3 \cdot AB$ to sustain its 3D structure. The distances between Al and B in BH_4^- narrowly range from 2.21 to 2.23 Å, while the distance between Al and B in BH_3 from AB is 2.31 Å. The distances between Al and H in BH_4^- are in the range of 1.65−1.81 Å, while the distances between Al and H in BH_3 range from 1.86 to 1.96 Å. The thermal decomposition of $Al(BH_4)_3 \cdot AB$ at 70 °C gave rise to the release of 2 Eq of H_2 (5 wt%), with a unique intermediate found in [6H + 1H] coordination of Al^{3+}. It is worth noting that the endothermic dehydrogenation of $Al(BH_4)_3 \cdot AB$ (39 kJ mol^{-1}) was achieved.

7. Other derivatives

7.1. $Mg(BH_4)_2 \cdot 2NH_3 \cdot NH_3BH_3$, $Mg(BH_4)_2 \cdot 2NH_3 \cdot AB$

$Mg(BH_4)_2 \cdot 2NH_3 \cdot AB$ was prepared by ball milling $Mg(BH_4)_2 \cdot 2NH_3$ with an equivalent AB [78]. It had a tetragonal cell in space group of $P4bm$ and the lattice parameters of a = 9.4643(8) Å and c = 5.5229(8) Å (Figure 26). Each Mg^{2+} is tetrahedrally coordinated by two BH_4^- with Mg-B distance of 2.30 Å and two NH_3 groups with Mg-N distance of 2.14 Å. NH_3 groups interact with their close BH_4^- and AB groups through the formation of BH···HN dihydrogen bonds(1.821-2.368 Å). Different from $Mg(BH_4)_2 \cdot 2AB$, $Mg(BH_4)_2 \cdot 2NH_3 \cdot AB$ exhibited significant depression of by-products and tremendously improved H_2 release. The onset dehydrogenation was reduced to 75 °C, and about 9.6 wt% H_2 could be released by 170 °C. Upon heating to 400 °C, a total amount of 13.8 wt% H_2 was desorbed.

For dehydrogenation improvement, $Zr(BH_4)_4 \cdot 8NH_3$ was ball milled with four equivalent AB. Although no new compound formed after ball milling and the subsequent heating treatment, it had an onset temperature at about 60 °C for dehydrogenation and could release 7.0 wt% H_2 at 100 °C in 45 min [81].

http://dx.doi.org/10.5772/61048

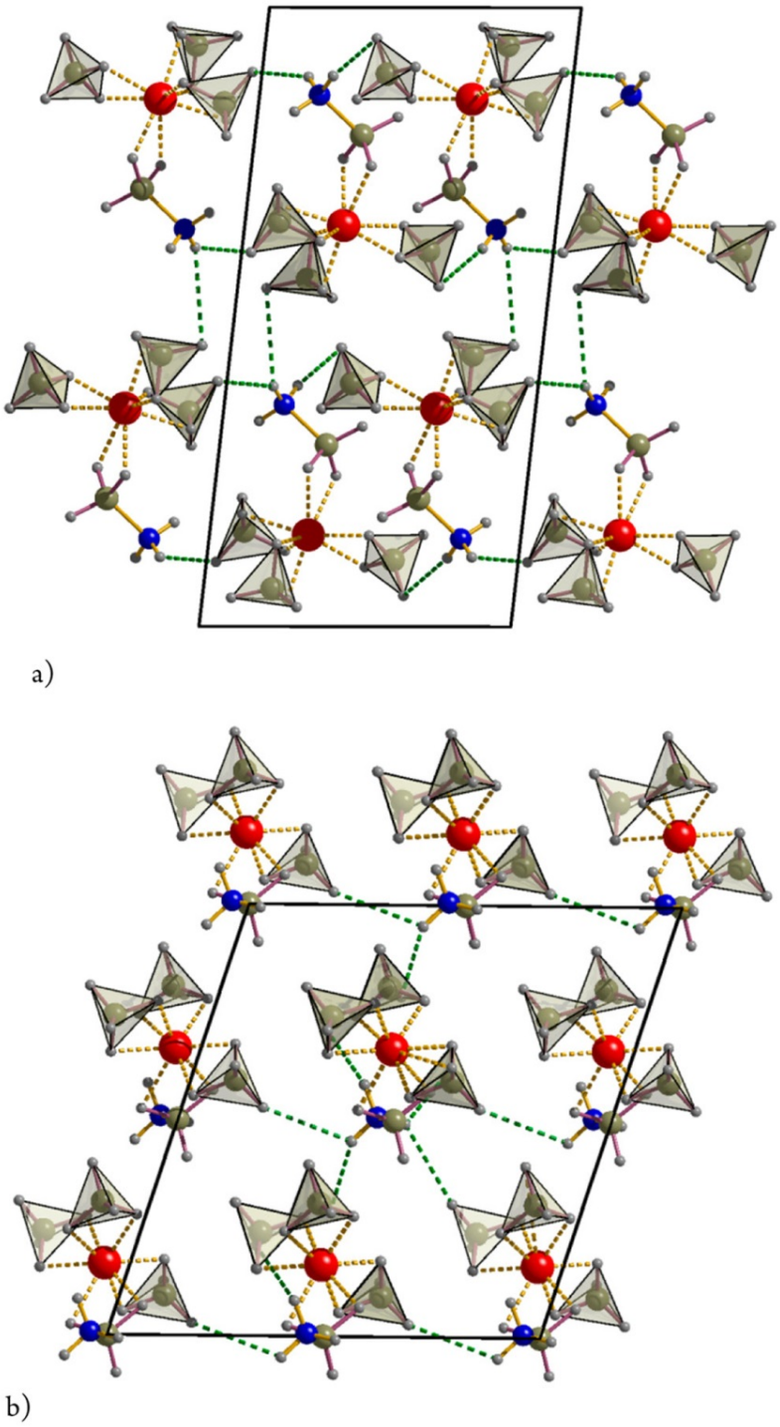

Figure 27. Crystal structure of $Al(BH_4)_3 \cdot AB$: (a) α-phase and (b) β-phase. Reproduced from Ref. [80] with permission.

7.2. $LiCa(NH_2)_3(BH_3)_2$

$LiCa(NH_2)_3(BH_3)_2$ was reported to be prepared by ball milling CaAB with an equivalent $LiNH_2$ [82]. Primary analysis showed that it crystallized in a monoclinic cell with lattice parameters of a = 7.3021 Å, b = 12.5513 Å, c = 5.0595 Å, and β = 120.98°. However, the detailed

crystal structure was not given. The onset temperature for dehydrogenation was at about 50 °C and a total amount of 6.8 wt% H_2 could be released exothermically upon heating to 300 °C, without the detectable borazine and diborane.

7.3. Sodium aminodiborane ($NaNH_2(BH_3)_2$)

$NaNH_2(BH_3)_2$ with an infrequent $NH_2(BH_3)_2^-$ anion was first reported by Girolami and coworkers in 2010 [83]. It was synthesized by the reduction of AB with excess Na in THF at room temperature and the following reflux. However, the target compound failed to isolate from the resulting THF adduct. In a very recent paper [84], solvent-free $NaNH_2(BH_3)_2$ was prepared by reacting $NaNH_2$ and two equivalent AB in THF. In a closed reactor, $NaNH_2(BH_3)_2$ could release 2 Eq of H_2 (6.0 wt%) at 271 °C, forming solid products of $NaBH_4$ and highly condensed polyborazylene.

7.4. $LiNH_2BH_3 \cdot LiBH_4$, $LiAB \cdot LiBH_4$

$LiAB \cdot LiBH_4$ was synthesized by ball milling LiAB with an equivalent $LiBH_4$ [85]. It was ascribed to an orthorhombic cell (space group *Pbca*) with lattice parameters of a = 9.2824(18) Å, b = 14.3092(28) Å, and c = 7.6194(12) Å. In $LiAB \cdot LiBH_4$ structure shown in Figure 28, alternative LiAB and $LiBH_4$ layers are stacked along the b axis. A strong interaction is resulting from the formed ionic bonds by Li^+ with $[NH_2BH_3]^-$ and BH_4^-. Li^+ has two tetrahedral coordination environments. One is surrounded by one BH_3 of $[NH_2BH_3]^-$ and three BH_4^-, while the other by one NH_2 of $[NH_2BH_3]^-$, one BH_4^-, and two BH_3 of $[NH_2BH_3]^-$. Furthermore, the BH···HN dihydrogen bondings range from 2.181 to 2.387 Å. However, the detailed dehydrogenation behavior of this compound was not given, although it had a similar process to 2LiAB/$LiBH_4$ reported in detail.

7.5. $M(BH_3NH_2BH_2NH_2BH_3)$, M = Li or Na

Preparation of $M(BH_3NH_2BH_2NH_2BH_3)$ (denoted as M(B3N2), M = Li or Na) was performed through a wet-chemical method in THF, according to the reaction: $MH + 3NH_3BH_3 \rightarrow M(BH_3NH_2BH_2NH_2BH_3) + NH_3 + 2H_2$ [86]. As stable white solids at room temperature, Li(B3N2) crystallizes in a tetragonal cell (space group $P\bar{4}2c$) with lattice parameters of a = 4.02(1) Å and c = 16.95(5) Å, while Na(B3N2) in a hexagonal cell (space group $P6_3/m$) of a = 4.3392(2) Å and c = 17.853(6) Å. Both crystal structures are shown in Figure 29. In Li(B3N2), each layer of Li^+ is linked by $(BH_3NH_2BH_2NH_2BH_3)^-$. Li^+ is tetrahedrally coordinated with four H atoms from terminal BH_3. The shortest distance between Li and H is 2.0 Å, and the average B-N bond length in $(BH_3NH_2BH_2NH_2BH_3)^-$ is about 1.59 Å. The twisty $(BH_3NH_2BH_2NH_2BH_3)^-$ were observed to lie along the c axis in Li(B3N2). It is worth noting that there is no interactions of BH···HN between neighboring $(BH_3NH_2BH_2NH_2BH_3)^-$. For the case of Na(B3N2) structure, there are some similarities to Li(B3N2), i.e., Na^+ layers perpendicular to the c axis separated by twisty $(BH_3NH_2BH_2NH_2BH_3)^-$. The most obvious difference is the fact that Na^+ is coordinated with eight H atoms with the closest Na-H distance of 2.22(9) Å. Upon heating, M(B3N2) decomposed exothermally into MBH_4 and H_2. As an example, Li(B3N2) had a weight loss of 5.0 wt% at 140 °C, contributed to hydrogen release without any ammonia or other impurities.

http://dx.doi.org/10.5772/61048

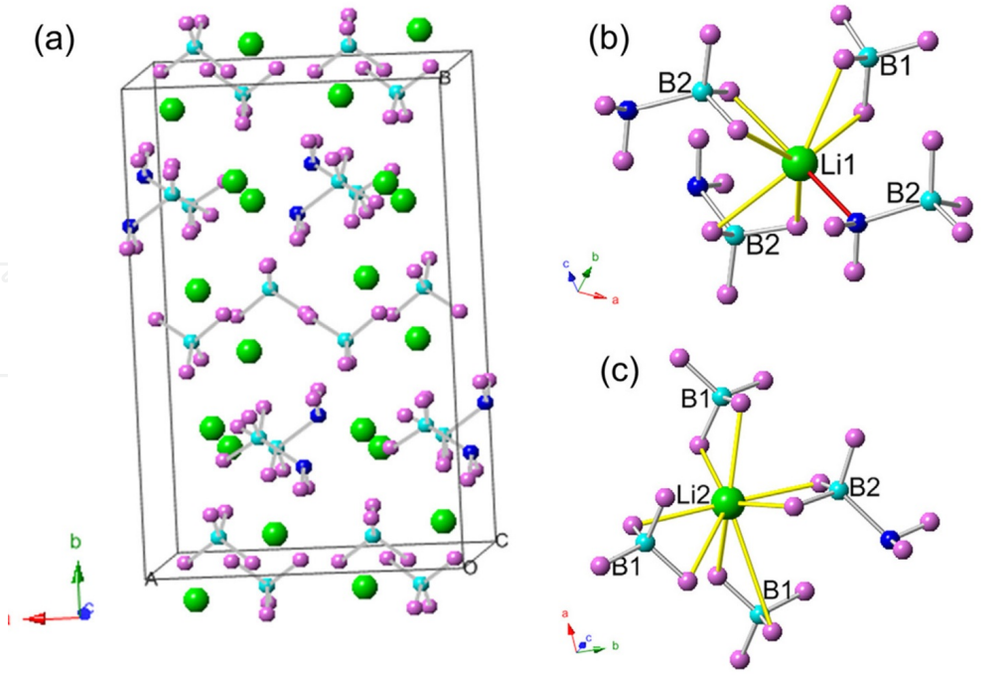

Figure 28. (a) Crystal structure of $LiAB \cdot LiBH_4$ and (b, c) Coordination of Li^+. Li: green spheres; N: blue spheres; B: cyan spheres; and H: pink spheres. Reproduced from Ref. [85] with permission.

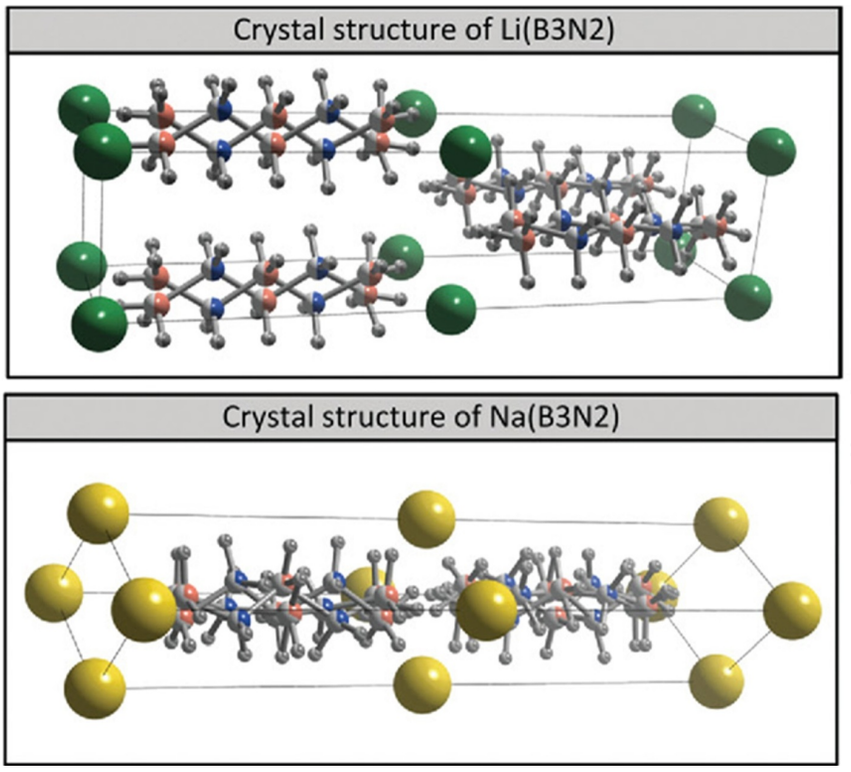

Figure 29. Crystal structure of Li(B3N2) and Na(B3N2): Li: green spheres; Na: yellow spheres; B: red spheres; N: blue spheres; and H: grey spheres. Reproduced from Ref. [86] with permission.

8. Conclusions

In this chapter, metal amidoboranes, metal borohydride-ammonia borane complexes, and metal amidoborane ammoniates as well as their derivatives were summarized with focus on their structures and dehydrogenation properties. In addition, nanoconfinement and nanocatalysis of AB for improving the dehydrogenation were also included. From scientific point of view, some new B–N-containing compounds and their crystal structures were reported, which enriches the chemistry of the scope of B and N elements. For the case of practical applications, the fast dehydrogenation rate at around 60 °C and the stability under 40 °C is one of the most important targets. Due to the difficulties in reversible hydrogenation of AB-related materials, off-board regeneration of spent fuel with high-energy efficiency is another issue to be solved. This would make it vitally important for altering the dehydrogenation thermodynamics from exothermicity to endothermicity. What is exciting is the fact that some cases of endothermic dehydrogenation were observed [60,62,80]. In this regard, it is indispensable for material design. That means that both a large number of experimental studies and the related theoretical calculations are urgently needed in the future. Moreover, catalytic modification should be considered for the dehydrogenation kinetics. In addition, how to eliminate the un-wanted by-products including ammonia, diborane, and borazine in the evolved hydrogen is also a critical issue, which needs special attention to be given because they are detrimental to proton exchange membrane (PEM) fuel cell, especially ammonia even with trace amount. As an example, there is a controversial debate of NaAB dehydrogenation for ammonia contamination [36,49,51]. Therefore, the mechanism for NH_3 formation during dehydrogenation is another task of further study.

Acknowledgements

The related research in this chapter was financially supported by the National Natural Science Foundation of China (51361006, 51401059, 51461010, 51361005, and 51371060), the Guangxi Natural Science Foundation (2014GXNSFAA118043, 2014GXNSFAA118333, 2013GXNSFBA019034, and 2013GXNSFBA019239), and the Guangxi University Research Project (YB2014132). This work was partially sponsored by Guangxi Collaborative Innovation Center of Structure and Property for New Energy Materials.

Author details

Hailiang Chu[1,2*], Shujun Qiu[1,2], Lixian Sun[1,2] and Fen Xu[1,2]

*Address all correspondence to: chuhailiang@guet.edu.cn

1 Guangxi Key Laboratory of Information Materials, Guilin University of Electronic Technology, Guilin, PR China

2 School of Materials Science and Engineering, Guilin University of Electronic Technology, Guilin, China

References

[1] Staubitz A, Robertson APM, Manners I. Ammonia-borane and related compounds as dihydrogen sources. Chemical Reviews 2010;110(7):4079-4124.

[2] Gao L, Li CYV, Yung H, Chan KY. A Functionalized MIL-101(Cr) metal-organic framework for enhanced hydrogen release from ammonia borane at low temperature. Chemical Communications 2013;49(90):10629-10631.

[3] Smythe NC, Gordon JC. Ammonia borane as a hydrogen carrier: dehydrogenation and regeneration. European Journal of Inorganic Chemistry 2010;4:509-521.

[4] Wolf G, Baumann J, Baitalow F, Hoffmann FP. Calorimetric process monitoring of thermal decomposition of B-N-H compounds. Thermochimica Acta 2000;343(1-2): 19-25.

[5] Hu MG, Geanangel RA, Wendlandt WW. The Thermal decomposition of ammonia borane. Thermochimica Acta 1978;23(2): 249-255.

[6] Gutowska A, Li L, Shin YS, Wang CMM, Li XHS, Linehan JC, Smith RS, Kay BD, Schmid B, Shaw W, Gutowski M, Autrey T. Nanoscaffold mediates hydrogen release and the reactivity of ammonia borane. Angewandte Chemie International Edition 2005;44(23):3578-3582.

[7] Feaver A, Sepehri S, Shamberger P, Stowe A, Autrey T, Cao G. Spectroscopic studies of dehydrogenation of ammonia borane in carbon cryogel. Journal of Physical Chemistry B 2007;111(51):7469-7472.

[8] Neiner D, Karkamkar A, Linehan JC, Arey B, Autrey T, Kauzlarich SM. Promotion of hydrogen release from ammonia borane with mechanically activated hexagonal boron nitride. Journal of Physical Chemistry C 2009;113(3):1098-1103.

[9] Bluhm ME, Bradley MG, Butterick R, Kusari U, Sneddon LG. Amineborane-based chemical hydrogen storage: enhanced ammonia borane dehydrogenation in ionic liquids. Journal of the American Chemical Society 2006;128(24):7748-7749.

[10] Zhang JS, Lee JW. Progress and prospects in thermolytic dehydrogenation of ammonia borane for mobile applications. Korean Journal of Chemical Engineering 2012;29(4):421-431.

[11] Denney MC, Pons V, Hebden TJ, Heinekey DM, Goldberg KI. Efficient catalysis of ammonia borane dehydrogenation. Journal of the American Chemical Society 2006;128(37):12048-12049.

[12] Zhang L, Tu Q, Chen X, Liu P. Nano metal catalysts in dehydrogenation of ammonia borane. Progress in Chemistry 2014;26(5):749-755.

[13] Zimmerman PM, Paul A, Zhang ZY, Musgrave CB. The role of free N-heterocyclic carbene (NHC) in the catalytic dehydrogenation of ammonia-borane in the nickel NHC system. Angewandte Chemie International Edition 2009;48(12):2201-2205.

[14] Zhao J, Shi J, Zhang X, Cheng F, Liang J, Tao Z, Chen J. A soft hydrogen storage material: poly(methyl acrylate)-confined ammonia borane with controllable dehydrogenation. Advanced Materials 2010;22(3):394-397.

[15] Chua YS, Chen P, Wu G, Xiong Z. Development of amidoboranes for hydrogen storage. Chemical Communications 2011;47(18):5116-5129.

[16] Wang K, Zhang J, Man T, Wu M, Chen C. Recent process and development of metal aminoborane. Chemistry—An Asian Journal 2013;8(11):1076-1089.

[17] Wolstenholme DJ, Titah JT, Che FN, Traboulsee KT, Flogeras J, McGrady GS. Homopolar dihydrogen bonding in alkali-metal amidoboranes and its implications for hydrogen storage. Journal of the American Chemical Society 2011;133(41):16598-16604.

[18] Luedtke AT, Autrey T. Hydrogen release studies of alkali metal amidoboranes. Inorganic Chemistry 2010;49(8):3905-3910.

[19] Jepsen LH, Ley MB, Lee YS, Cho YW, Dornheim M, Jensen JO, Filinchuk Y, Jørgensen JE, Besenbacher F, Jensen TR. Boron-nitrogen based hydrides and reactive composites for hydrogen storage. Materials Today 2014;17(3):129-135.

[20] Moussa G, Moury R, Demirci UB, Şener T, Miele P. Boron-based hydrides for chemical hydrogen storage. International Journal of Energy Research 2013;37(8):825-842.

[21] Furukawa H, Cordova KE, O'Keeffe M, Yaghi OM. The chemistry and applications of metal-organic frameworks. Science 2013;341(6149):1230444.

[22] Zhou HC, Long JR, Yaghi OM. Introduction to metal-organic frameworks. Chemical Reviews 2012;112(2):673-674.

[23] Li Z, Zhu G, Lu G, Qiu S, Yao X. Ammonia borane confined by a metal-organic framework for chemical hydrogen storage: enhancing kinetics and eliminating ammonia. Journal of the American Chemical Society 2010;132(5):1490-1491.

[24] Gadipelli S, Ford J, Zhou W, Wu H, Udovic TJ, Yildirim T. Nanoconfinement and catalytic dehydrogenation of ammonia borane by magnesium-metal-organic-framework-74. Chemistry—A European Journal 2011;17(22):6043-6047.

[25] Si X, Sun L, Xu F, Jiao C, Li F, Liu S, Zhang J, Song L, Jiang C, Wang S, Liu Y, Sawada Y. Improved hydrogen desorption properties of ammonia borane by Ni-modified metal-organic frameworks. International Journal of Hydrogen Energy 2011;36(11):6698-6704.

[26] Cheng F, Ma H, Li Y, Chen J. $Ni_{1-x}Pt_x$ (x = 0-0.12) hollow spheres as catalysts for hydrogen generation from ammonia borane. Inorganic Chemistry 2007;46(3):788-794.

[27] He T, Xiong Z, Wu G, Chu H, Wu C, Zhang T, Chen P. Nanosized Co- and Ni-catalyzed ammonia borane for hydrogen storage. Chemistry of Materials 2009;21(11): 2315-2318.

[28] He T, Wang J, Wu G, Kim H, Proffen T, Wu A, Li W, Liu T, Xiong Z, Wu C, Chu H, Guo J, Autrey T, Zhang T, Chen P. Growth of Crystalline polyaminoborane through catalytic dehydrogenation of ammonia borane on FeB nanoalloy. Chemistry—A European Journal 2010;16(43):12814-12817.

[29] He T, Wang J, Liu T, Wu G, Xiong Z, Yin J, Chu H, Zhang T, Chen P. Quasi in situ Mössbauer and XAS studies on FeB nanoalloy for heterogeneous catalytic dehydrogenation of ammonia borane. Catalysis Today 2011;170(1):69-75.

[30] Li L, Yao X, Sun C, Du A, Cheng L, Zhu Z, Yu C, Zou J, Smith SC, Wang P, Cheng H, Frost RL, Lu G. Lithium-catalyzed dehydrogenation of ammonia borane within mesoporous carbon framework for chemical hydrogen storage. Advanced Functional Materials 2009;19(2):265-271.

[31] Li Y, Song P, Zheng J, Li X. Promoted H_2 generation from NH_3BH_3 thermal dehydrogenation catalyzed by metal-organic framework based catalysts. Chemistry—A European Journal 2010;16(35):10887-10892.

[32] Li S, Guo Y, Sun W, Sun D, Yu X. Platinum nanoparticle functionalized CNTs as nanoscaffolds and catalysts to enhance the dehydrogenation of ammonia-borane. Journal of Physical Chemistry C 2010;114(49):21885-21890.

[33] Xin G, Yang J, Li W, Zheng J, Li X. Catalytic thermal decomposition of ammonia-borane by well-dispersed metal nanoparticles on mesoporous substrates prepared by magnetron sputtering. European Journal of Inorganic Chemistry 2012;34: 5722-5728.

[34] Schlesinger HI, Burg AB. Hydrides of Boron. VIII. The structure of the diammoniate of diborane and its relation to the structure of diborane. Journal of the American Chemical Society 1938;60(2):290-299.

[35] Myers AG, Yang BH, David KJ. Lithium amidotrihydroborate, a powerful new reductant. Transformation of tertiary amides to primary alcohols. Tetrahedron Letters 1996;37(21):3623-3626.

[36] Xiong Z, Yong CK, Wu G, Chen P, Shaw W, Karkamkar A, Autrey T, Jones MO, Johnson SR, Edwards PP, David WIF. High-capacity hydrogen storage in lithium and sodium amidoboranes. Nature Materials 2008;7:138-141.

[37] Kang X, Fang Z, Kong L, Cheng H, Yao X, Lu G, Wang P. Ammonia borane destabilized by lithium hydride: an advanced on-board hydrogen storage material. Advanced Materials 2008;20(14):2756-2759.

[38] Wu H, Zhou W, Yildirim T. Alkali and alkaline-earth metal amidoboranes: structure, crystal chemistry, and hydrogen storage properties. Journal of the American Chemical Society 2008;130(44):14834-14839.

[39] Diyabalanage HVK, Shrestha RP, Semelsberger TA, Scott BL, Bowden ME, Davis BL, Burrell AK. Calcium amidotrihydroborate: a hydrogen storage material. Angewandte Chemie International Edition 2007;46(47):8995-8997.

[40] Diyabalanage HVK, Nakagawa T, Shrestha RP, Semelsberger TA, Davis BL, Scott BL, Burrell AK, David WIF, Ryan KR, Jones MO, Edwards PP. Potassium(I) amidotrihydroborate: structure and hydrogen release. Journal of the American Chemical Society 2010;132(34):11836-11837.

[41] Zhang Q, Tang C, Fang C, Fang F, Sun D, Ouyang L, Zhu M. Synthesis, crystal structure, and thermal decomposition of strontium amidoborane. Journal of Physical Chemistry C 2010;114(3):1709-1714.

[42] Genova RV, Fijalkowski KJ, Budzianowski A, Grochala W. Towards $Y(NH_2BH_3)_3$: probing hydrogen storage properties of YX_3/MNH_2BH_3 (X = F, Cl; M= Li, Na) and $YH_{x\sim3}/NH_3BH_3$ composites. Journal of Alloys and Compounds 2010;499(2):144-148.

[43] Lu J, Fang Z. Dehydrogenation of a combined $LiAlH_4/LiNH_2$ system. Journal of Physical Chemistry B 2005;109(44): 20830-20834.

[44] Chen P, Xiong Z, Luo J, Lin J, Tan K. Interaction between lithium amide and lithium hydride. Journal of Physical Chemistry B 2003;107(39):10967-10970.

[45] Xiong Z, Wu G, Hu J, Chen P. Ternary Imides for hydrogen storage. Advanced Materials 2004;16(17):1522-1525.

[46] Hughes EW. The crystal structure of ammonia-borane, H_3NBH_3. Journal of the American Chemical Society 1956;78(2):502-503.

[47] Bowden ME, Gainsford GJ, Robinson WT. Room-temperature structure of ammonia borane. Australian Journal of Chemistry 2007;60(3):149-153.

[48] Xiong Z, Chua YS, Wu G, Xu W, Chen P, Shaw W, Karkamkar A, Linehan J, Smurthwaite T, Autrey T. Interaction of lithium hydride and ammonia borane in THF. Chemical Communications 2008;43:5595-5597.

[49] Xia G, Chen J, Sun W, Tan Y, Guo Z, Liu H, Yu X. Well-dispersed lithium amidoborane nanoparticles through nanoreactor engineering for improved hydrogen release. Nanoscale 2014;6(21):12333-12339.

[50] Xiong Z, Wu G, Chua YS, Hu J, He T, Xu W, Chen P. Synthesis of sodium amidoborane ($NaNH_2BH_3$) for hydrogen production. Energy and Environmental Science 2008;1(3):360-363.

[51] Shimoda K, Zhang Y, Ichikawa T, Miyaoka H, Kojima Y. Solid state NMR study on the thermal decomposition pathway of sodium amidoborane $NaNH_2BH_3$. Journal of Materials Chemistry 2011;21(8):2609-2615.

[52] Fijałkowski KJ, Grochala W. Substantial emission of NH_3 during thermal decomposition of sodium amidoborane, $NaNH_2BH_3$. Journal of Materials Chemistry 2009;19(14):2043-2050.

[53] Wu C, Wu G, Xiong Z, David WIF, Ryan KR, Jones MO, Edwards PP, Chu H, Chen P. Stepwise phase transition in the formation of lithium amidoborane. Inorganic Chemistry 2010;49(9):4319-4323.

[54] Wu C, Wu G, Xiong Z, Han X, Chu H, He T, Chen P. $LiNH_2BH_3 \cdot NH_3BH_3$: structure and hydrogen storage properties. Chemistry of Materials 2010;22(1):3-5.

[55] Luo J, Kang X, Wang P. Synthesis, formation mechanism, and dehydrogenation properties of the long-sought $Mg(NH_2BH_3)_2$ compound. Energy and Environmental Science 2013;6(3):1018-1025.

[56] Spielmann J, Jansen G, Bandmann H, Harder S. Calcium amidoborane hydrogen storage materials: crystal structures of decomposition products. Angewandte Chemie International Edition 2008;47(33):6290-6295.

[57] He T, Wang J, Chen Z, Wu A, Wu G, Yin J, Chu H, Xiong Z, Zhang T, Chen P. Metathesis of alkali-metal amidoborane and $FeCl_3$ in THF. Journal of Materials Chemistry 2012;22(15):7478-7483.

[58] Fijalkowski KJ, Genova RV, Filinchuk Y, Budzianowski A, Derzsi M, Jaroń T, Leszczynski PJ, Grochala W. $Na[Li(NH_2BH_3)_2]$—the first mixed-cation amidoborane with unusual crystal structure. Dalton Transactions 2011;40(17):4407-4413.

[59] Li W, Miao L, Scheicher RH, Xiong Z, Wu G, Araújo CM, Blomqvist A, Ahuja R, Feng Y, Chen P. Li-Na ternary amidoborane for hydrogen storage: experimental and first-principles study. Dalton Transactions 2012;41(16):4754-4764.

[60] Kang X, Luo J, Zhang Q, Wang P. Combined formation and decomposition of dual-metal amidoborane $NaMg(NH_2BH_3)_3$ for high-performance hydrogen storage. Dalton Transactions 2011;40(15):3799-3801.

[61] Wu H, Zhou W, Pinkerton FE, Meyer MS, Yao QR, Gadipelli S, Udovic TJ, Yildirim T, Rush JJ. Sodium magnesium amidoborane: the first mixed-metal amidoborane. Chemical Communications 2011;47(14):4102-4104.

[62] Chua YS, Li W, Wu G, Xiong Z, Chen P. From exothermic to endothermic dehydrogenation—interaction of monoammoniate of magnesium amidoborane and metal hydrides. Chemistry of Materials 2012;24(18):3574-3581.

[63] Xia G, Tan Y, Chen X, Guo Z, Liu H, Yu X. Mixed-metal (Li, Al) amidoborane: synthesis and enhanced hydrogen storage properties. Journal of Materials Chemistry A 2013;1(5):1810-1820.

[64] Nakagawa Y, Ikarashi Y, Isobe S, Hino S, Ohnuki S. Ammonia borane-metal alanate composites: hydrogen desorption properties and decomposition processes. RSC Advances 2014;4(40):20626-20631.

[65] Sorensen RZ, Hummelshoj JS, Klerke A, Reves JB, Vegge T, Norskov JK, Christensen CH. Indirect, reversible high-density hydrogen storage in compact metal ammine salts. Journal of the American Chemical Society 2008;130(27):8660-8668.

[66] Christensen CH, Sørensen RZ, Johannessen T, Quaade UJ, Honkala K, Elmøe TD, Køhler R, Nørskov JK. Metal ammine complexes for hydrogen storage. Journal of Materials Chemistry 2005;15(38):4106-4108.

[67] Lin R, Liu Y, Gao M, Wang J, Ge H, Pan H. Investigation on performances of the novel ammonia-based hydrogen storage material $CaCl_2$. Journal of Inorganic Materials 2008;23(5):1059-1063.

[68] Soloveichik G, Her JH, Stephens PW, Gao Y, Rijssenbeek J, Andrus M, Zhao JC. Ammine magnesium borohydride complex as a new material for hydrogen storage: structure and properties of $Mg(BH_4)_2 \cdot 2NH_3$. Inorganic Chemistry 2008;47(10): 4290-4298.

[69] Chu H, Wu G, Xiong Z, Guo J, He T, Chen P. Structure and hydrogen storage properties of calcium borohydride diammoniate. Chemistry of Materials 2010;22(21): 6021-6028.

[70] Graham KR, Kemmitt T, Bowden ME. High capacity hydrogen storage in a hybrid ammonia borane-lithium amide material. Energy and Environmental Science 2009;2(6):706-710.

[71] Xia G, Yu X, Guo Y, Wu Z, Yang C, Liu H, Dou S. Amminelithium amidoborane $[Li(NH_3)NH_2BH_3]$: a new coordination compound with favorable dehydrogenation characteristics. Chemistry—A European Journal 2010;16(12):3763-3769.

[72] Chua YS, Wu G, Xiong Z, He T, Chen P. Calcium amidoborane ammoniate-synthesis, structure, and hydrogen storage properties. Chemistry of Materials 2009;21(20): 4899-4904.

[73] Chua YS, Wu H, Zhou W, Udovic TJ, Wu G, Xiong Z, Wong MW, Chen P. Monoammoniate of calcium amidoborane: synthesis, structure, and hydrogen-storage properties. Inorganic Chemistry 2012;51(3):1599-1603.

[74] Chua YS, Wu G, Xiong Z, Karkamkar A, Guo J, Jian MX, Wong MW, Autrey T, Chen P. Synthesis, structure and dehydrogenation of magnesium amidoborane monoammoniate. Chemical Communications 2010;46(31):5752-5754.

[75] Wu H, Zhou W, Pinkerton FE, Meyer MS, Srinivas G, Yildirim T, Udovic TJ, Rush JJ. A new family of metal borohydride ammonia borane complexes: synthesis, structures, and hydrogen storage properties. Journal of Materials Chemistry 2010;20(31): 6550-6556.

[76] Jepsen LH, Skibsted J, Jensen TR. Investigations of the thermal decomposition of MBH_4-$2NH_3BH_3$, M = Na, K. Journal of Alloys and Compounds 2013;580(S1):S287-S291.

[77] Luo J, Wu H, Zhou W, Kang X, Fang Z, Wang P. $LiBH_4 \cdot NH_3BH_3$: a new lithium borohydride ammonia borane compound with a novel structure and favorable hydrogen storage properties. International Journal of Hydrogen Energy 2012;37(14): 10750-10757.

[78] Chen X, Yuan F, Gu Q, Yu X. Synthesis, structures and hydrogen storage properties of two new H-enriched compounds: $Mg(BH_4)_2(NH_3BH_3)_2$ and $Mg(BH_4)_2 \cdot (NH_3)_2(NH_3BH_3)$. Dalton Transactions 2013;42(40):14365-14368.

[79] Jepsen LH, Ban V, Møller KT, Lee YS, Cho YW, Besenbacher F, Filinchuk Y, Skibsted J, Jensen TR. Synthesis, crystal structure, thermal decomposition, and ^{11}B MAS NMR characterization of $Mg(BH_4)_2(NH_3BH_3)_2$. Journal of Physical Chemistry C 2014;118(23):12141-12153.

[80] Dovgaliuk I, Duff CSL, Robeyns K, Devillers M, Filinchuk Y. Mild dehydrogenation of ammonia borane complexed with aluminum borohydride. Chemistry of Materials 2015;27(3):768-777.

[81] Huang J, Tan Y, Gu Q, Ouyang L, Yu X, Zhu M. Ammonia borane modified zirconium borohydride octaammoniate with enhanced dehydrogenation properties. Journal of Materials Chemistry A 2015;3(10):5299-5304.

[82] Liu B, Chua YS, Wu G, Xiong Z, Chen P. Synthesis and dehydrogenation of Li-$Ca(NH_2)_3(BH_3)_2$. International Journal of Hydrogen Energy 2012;37(11):9076-9081.

[83] Daly SR, Bellott BJ, Kim DY, Girolami GS. Synthesis of the long-sought unsubstituted aminodiboranate $Na(H_3B\text{-}NH_2\text{-}BH_3)$ and its N-Alkyl analogs. Journal of the American Chemical Society 2010;132(21):7254-7255.

[84] Chen W, Huang Z, Wu G, Chen P. New synthetic procedure for $NaNH_2(BH_3)_2$ and evaluation of its hydrogen storage properties. Science China Chemistry 2015;58(1): 169-173.

[85] Chen J, He T, Wu G, Xiong Z, Chen P. Synthesis and hydrogen storage properties of lithium borohydride amidoborane complex. International Journal of Hydrogen Energy 2013;38(25):10944-10949.

[86] Fijalkowski KJ, Jaroń T, Leszczyński PJ, Magos-Palasyuk E, Palasyuk T, Cyrańskic MK, Grochala W. $M(BH_3NH_2BH_2NH_2BH_3)$—the missing link in the mechanism of the thermal decomposition of light alkali metal amidoboranes. Physical Chemistry Chemical Physics 2014;16(42):23340-23346.

IntechOpen